INCREASING REFLECTION COHERENCY THROUGH IMPROVED STATIC CORRECTIONS: AN ITERATIVE TOMOGRAPHIC APPROACH

BY

Lindsay M. Mayer

Submitted to the graduate degree program in Geology
and the Graduate Faculty of the University of Kansas
in partial fulfillment of the requirements for the degree of
Master of Science.

_____
Dr. Rick D. Miller, Chair

Committee members* _____*
Dr. Ross A. Black

_____*
Dr. Diane Kamola

Date defended:_____

The Thesis Committee for Lindsay M. Mayer certifies
that this is the approved Version of the following thesis:

INCREASING REFLECTION COHERENCY THROUGH IMPROVED STATIC CORRECTIONS: AN ITERATIVE TOMOGRAPHIC APPROACH

Committee:

_____
Dr. Rick D. Miller, Chair

_____
Dr. Ross A. Black

_____
Dr. Diane Kamola

Date approved:_____

Abstract

Computation and application of statics corrections have always been problematic on CMP reflection data, especially in highly weathered and structurally altered environments. Tomographic estimation of the velocity field is a severely underdetermined problem, only to be exacerbated by the lack of *a priori* information of the survey site. Statistically driven static techniques are sometimes considered unplausible for specific subsurface conditions rendering them only aesthetically useful to the final stacked section. Using turning-ray tomography to make static corrections (tomostatics) and iteratively developing the best tomographic model will ultimately optimize the static correction for each source and receiver station. Cross-correlation statics routines guided the selection of the best initial model, monitoring changes in specific near-surface reflections during iterative application of tomostatics. Combining statistical techniques with geologically based models of the subsurface increases the total reflection coherency and accuracy of the final stacked section.

Table of Contents **Page**

List of Figures **Page**

List of Tables **Page**

1. Introduction

Lateral inhomogeneities in the near-surface have been recognized as the source of irregular seismic travel times since the earliest reflection surveys were conducted (Cox, 1999). These irregular travel time arrivals, termed statics, result in destructive interference during common-midpoint (CMP) data processing. Time shifts applied to the seismic data to compensate for these lateral inhomogeneities in the weathered interval are intended to adjust all time measurements to a flat plane below the weathered layer (Sheriff, 1991). Effectively the static correction removes all variability in surface topography and material velocity above a designated datum. Static corrections are applied to compensate for variability that inhibits production of an accurate zero offset reflection image of the subsurface.

Conventional techniques used to meet the statics correction objective, such as defining the weathered layer velocity using refraction methods, have had limited success in areas with extreme lateral variations in the physical parameters of the sediment (Pugin and Pullan, 2000). Additionally, the lack of *a priori* information about the near-surface (i.e. boreholes, depth to bedrock) in most seismic studies make statics corrections using first-arrivals problematic (Ivanov et al., 2005a). In areas with structurally altered bedrock and severely heterogeneous weathered layers, statics corrections can be orders of magnitude greater than the structures being imaged (Miller, 2007). Promising methods have been developed recently to define the velocity function of the near-surface in the presence of these large velocity irregularities (Zhu and McMechan, 1988). If a detailed velocity function can be

accurately determined and applied, even statics problems from unconsolidated, poorly sorted overburden in extremely difficult areas can be eliminated (de Amorim et al., 1987, Zhu et al., 1992).

Iterating between statics correction and velocity modeling should ultimately allow selection of the best detailed velocity model for a particular geology. Using reflection coherency present in the data itself as a gauge in selecting this optimum velocity model and therefore static correction, site-specific information can be used to guide convergence to the "best" velocity function. In this study a new iterative static approach is developed and tested on two field areas: a geologically uncomplicated Permian succession covered by Quaternary alluvial deposits near Hutchinson, Kansas, and a geologically complicated Ordovician system with Tertiary/Quaternary colluvial infill deposits near Winnemucca, Nevada.

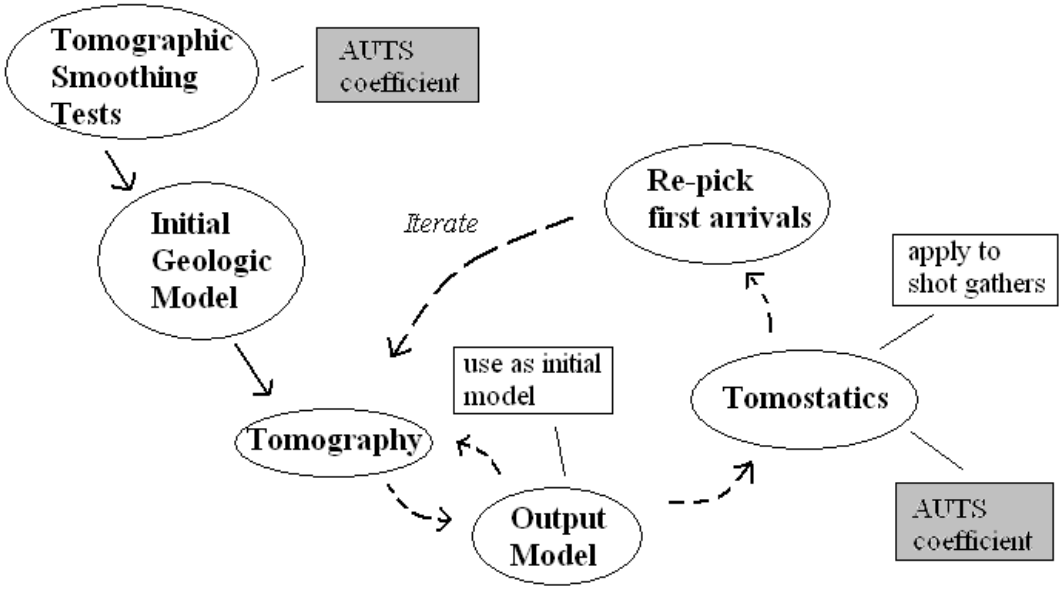

Figure 1.1- Proposed processing flow for the iterative tomostatic approach. The dashed arrows represent steps that are repeated and the solid arrows represent input to the process that is only performed once. The tomographic smoothing tests decide the best velocity model, and each following iteration of tomography is damped according to this model.

2. Background

Common to all statics methods applied to reflection data are assumptions about the subsurface. These assumptions, such as continuous reflectors and laterally homogeneous layering, are critical to application of conventional statics routines. In most near-surface seismic studies there is minimal *a priori* information about the subsurface from boreholes (Pugin and Pullan, 2000), or other types of geophysical data making the near-surface velocity problem extremely underdetermined[1] and usually debilitating to conventional statics techniques. In this section, conventional statics routines and their associated assumptions will be reviewed.

2.1 Conventional Statics Methods

There are three main types of static corrections in traditional seismic reflection processing: datum or refraction statics, surface-consistent statics, and residual or trim statics (Yilmaz, 1987; Pugin and Pullan, 2000). In most cases these three methods will reduce trace-to-trace reflection time variability due to changes in the near-surface that degrade the final-stacked section. The latter two techniques make critical assumptions about wavelet characteristics that can be violated in highly weathered, structurally altered environments where S/N ratio[2] is low. The first parameter to be considered and accounted for through statics corrections in the seismic reflection processing flow is topographic changes along a seismic survey line (Cox, 1999).

[1] An underdetermined system contains more unknowns than equations (Sheriff, 2002).
[2] The ratio of the energy from the signal to all remaining energy (Sheriff, 2002).

Surface elevation is the easiest information to gather along a survey line and the severity of topographic relief is immediately known during the acquisition of seismic data. Static variations with wavelengths longer than the spread length in the seismic gather are referred to as long-wavelength variations (low-spatial-frequency), and are primarily associated with major topographic changes along a survey line (Pugin and Pullan, 2000). Typically datum static corrections are used to resolve these long-wavelength variations. If these are ignored during processing, they can appear as artificial structures in the final stacked section (Figure 2.1.1) (Cox, 1999).

Datum static corrections refer to any correction with reference to a "datum". Conventionally the datum is selected at a time below the weathered and sub-weathered layers, where the time correction is based on a replacement velocity calculated for the "weathered" interval. The objective of this correction is to adjust the reflection arrival times to what would have been observed if all measurements had been made along the datum plane with the weathering or low-velocity material removed (Figure 2.1.2) (Sheriff, 1991). A replacement velocity is used to calculate the datum statics correction and must be accurate to successfully account for the weathered layer.

The most widely used methods for characterizing near-surface velocity structure for datum statics corrections are refraction and uphole surveys (Cox, 1999). Uphole surveys generate one-way travel times that translate into a more reliable velocity model at the measurement location, however, depending on the site may not easily extrapolate across the reflection survey line. Refractions can be interpreted

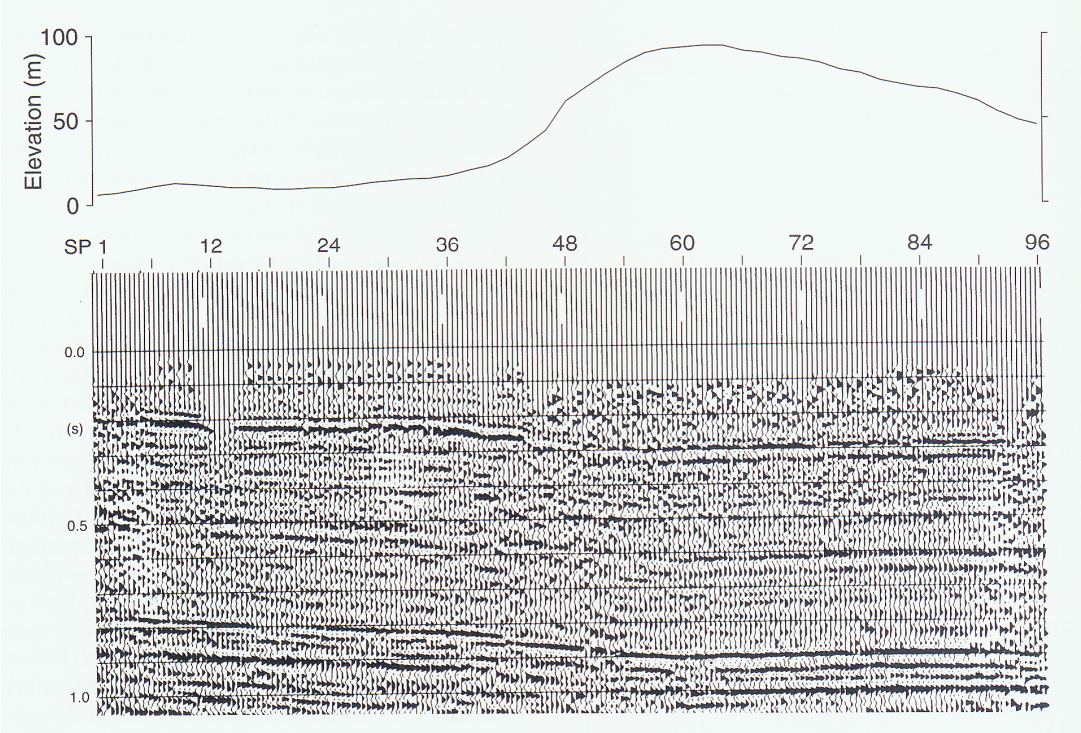

Figure 2.1.1- Stacked data without datum static corrections. Survey line contains a topographic feature with about 80 m of relief (After Cox, 1999).

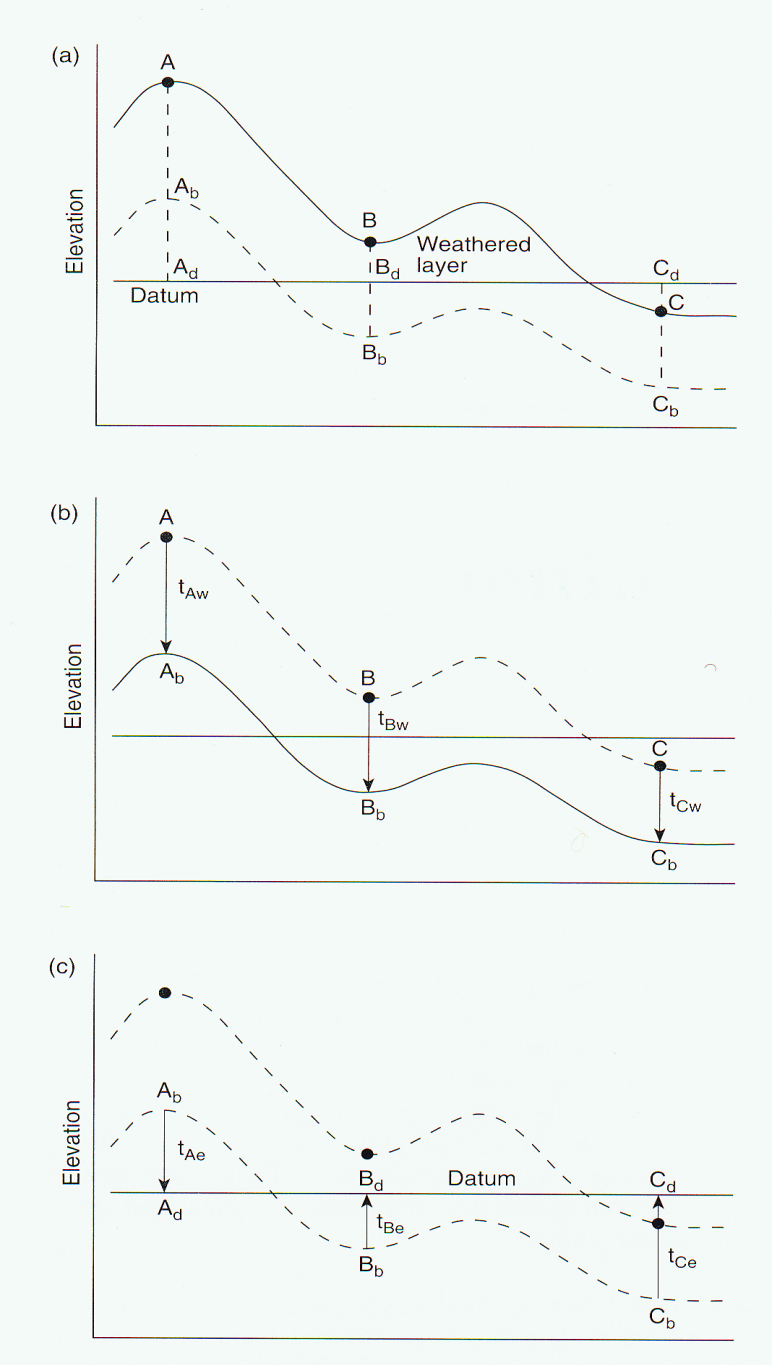

Figure 2.1.2- An example of static corrections from velocity model **(a)** to a flat datum at three locations A, B, and C. The time correction includes one for the weathering layer (t_{Aw}, t_{Bw}, t_{Cw}) **(b)** and one for the elevation (t_{Ae}, t_{Be}, t_{Ce}) **(c)** (after Cox, 1999). The weathering correction **(b)** is positive in time (shift down) for all three locations. The elevation correction **(c)** is positive for location A but negative (shift up) for locations B and C.

from reflection shot gathers making it a cheaper and generally easier option, however may not provide the accuracy needed to compensate for the weathered interval. Consequently, many methods for refraction analysis have been developed.

Interpretation of the refractions and calculation of RMS velocities and layer thickness can be done in many ways: the Intercept-Time method, the Plus-Minus method, the Method of Differences, the Generalized Reciprocal Method (GRM), Blondeau Method, and the Gardner Method among others (Hagedoorn, 1959; Edge and Laby, 1931; Palmer, 1980; Dobrin, 1976; Gardner, 1939a, b). These methods assume constant lateral velocity, relatively simple structure, and increasing velocity with depth. In mature topography, where the surface profile gives no indication of the extreme variations in the near-surface, all these assumptions are violated (Cox, 1999).

A technique often used following application of datum static corrections to address remaining medium and short wavelength time shifts is called residual statics (Taner, 1998). Residual statics encompasses two statistically controlled methods to correct "chatter" relative to the datum plane: surface-consistent statics and trim statics (Hileman et al., 1968; Garotta and Michon, 1968; Irvine and Worley, 1969; Disher and Naquin, 1970; Sherwood and Donaldson, 1970; Taner et al., 1974). Variations in near-surface velocity conditions cause medium and short wavelength statics (high-spatial-frequency), which can be defined as time variability with wavelengths on the order of a receiver spread and receiver interval respectively. The quality of the final stacked section can be severely degraded by these statics if uncorrected, but they do

not strongly affect structural interpretation, which are ideally addressed with datum statics (Pugin and Pullan, 2000).

The term “surface consistent” is used to express time delay static corrections originating directly below, and unique to, each source and receiver station regardless of the raypath (Taner et al, 1974). Taner et al. (1974) goes onto define source and receiver statics as time delays introduced near the source by the downgoing wavefield and delays introduced near the receiver from the upcoming wavefield.

The surface-consistent method mathematically examines consistency in reflection wavelets using the cross-correlations of each trace of a common midpoint (CMP) with a pilot trace formed by combining a number of CMP’s. The objective is to measure relative time shifts based on common receiver and shot locations (Figure 2.1.3). The time shift is calculated on traces that have undergone normal-moveout correction (NMO) to simulate vertical incidence. The correlation is constrained to a selected gate with a resulting optimum shift for each trace catalogued in a table according to shot and receiver location (Figure 2.1.4) (Hileman et al., 1968). A time shift that aligns all primary reflections within a CMP gather (Figure 2.1.5) can be achieved by shifting each trace until the cross-correlation coefficient is maximized (Taner et. al, 1974). The time correction calculation is statistically governed by the size of the gate, target reflector, number of CMP’s summed to make the pilot trace, and the static limit. The statics routine is iterated with velocity analysis to optimize the velocity solution and therefore the static solution (Taner et al., 1974).

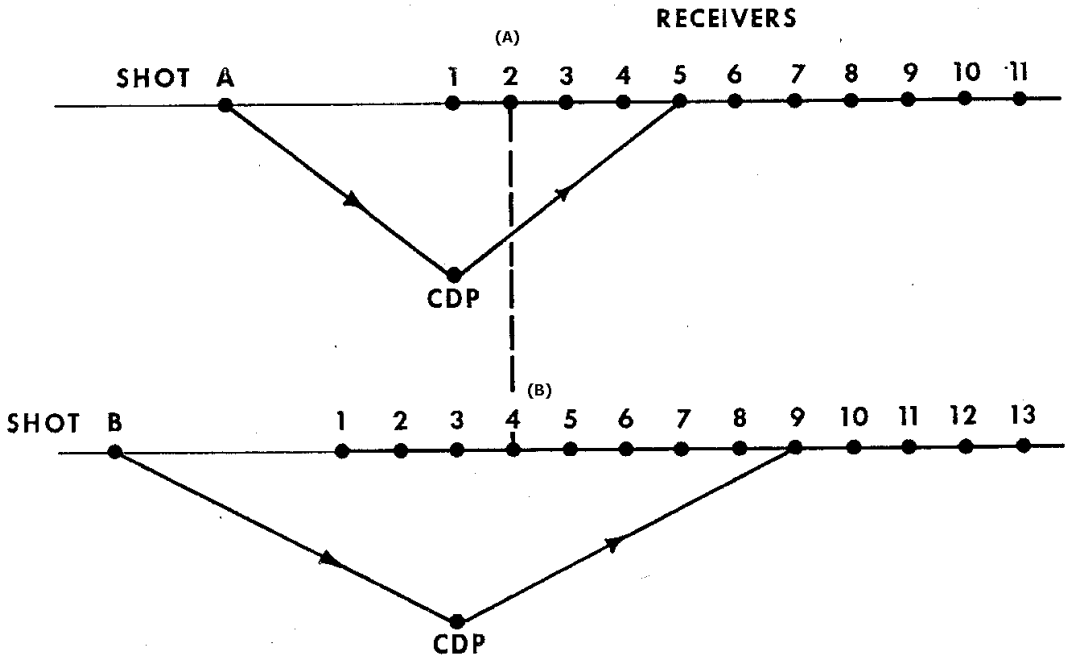

Figure 2.1.3-Diagram of shot and receiver relationships within a CDP gather for surface consistent statics corrections. Receiver 2 **(A)** in the top diagram and receiver 4 **(B)** in the bottom diagram will have the same receiver static correction regardless of raypath, but different shot static corrections. This is a CDP configuration for 6-fold data (after Hileman et al., 1968).

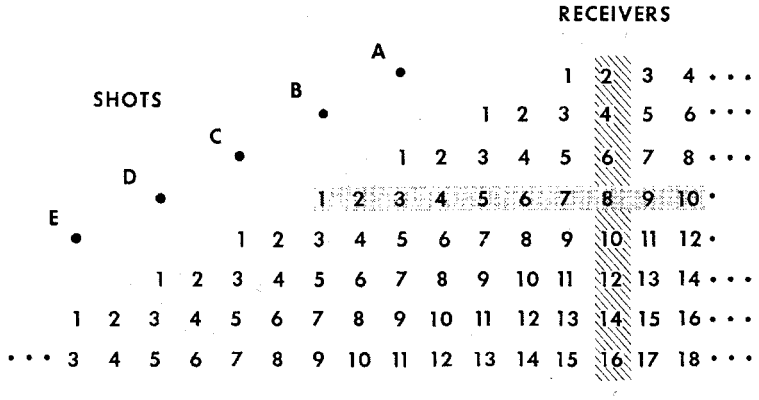

Figure 2.1.4- Diagram illustrating computation array for a 6-fold shooting geometry with surface consistent statics. Time shifts associated with certain receivers are in columns and time shifts of shots are in rows (after Hileman at al., 1968).

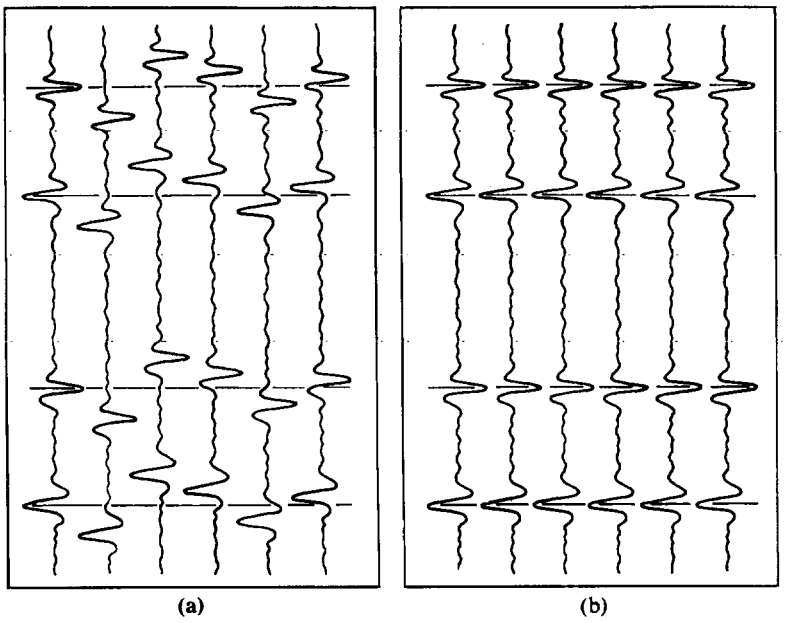

Figure 2.1.5- A CDP gather before alignment of traces with statics (a), and after surface consistent cross-correlation technique (b) (after Taner et al., 1974).

Surface consistent static corrections are estimated in the CMP domain, therefore cannot be uniquely attributed or correlated to geologic dip or structure (Hileman et al., 1968). Also alignment of traces to estimate static relies on continuous reflections with uniform phase and no wavelet interference due to tuning or excessive noise, conditions that rarely exist in data with a poor S/N ratio (Figure 2.1.5)(Taner, 1998). In noisy data with substantial statics problems the cross-correlation routine rarely picks the appropriate reflection peaks based on the input parameters of the processor (Figure 2.1.6). If not properly constrained, this process can diverge from reality, guided by the probability function, producing results with no substantial relationship to geology.

Trim statics is traditionally the final step in a statics routine. It is intended to eliminate any lingering mathematically unrelatable time shifts left after surface-consistent statics and the final NMO velocity correction. The correlation routine is similar to the approach used for surface-consistent statics, correlating a pilot trace produced from summing several CMP's with the individual traces within a CMP. The difference is trim statics corrects for calculated static of each trace automatically based on given thresholds without regard to receiver or source locations. This routine tries to simply align traces and in the extreme case can be applied so that it flattens reflections regardless of reflector geometry.

2.2 Refraction Tomography

Statics irregularities in traces and near-surface velocity variability are inherently related, and it can be argued that statics, as a physical phenomenon, does

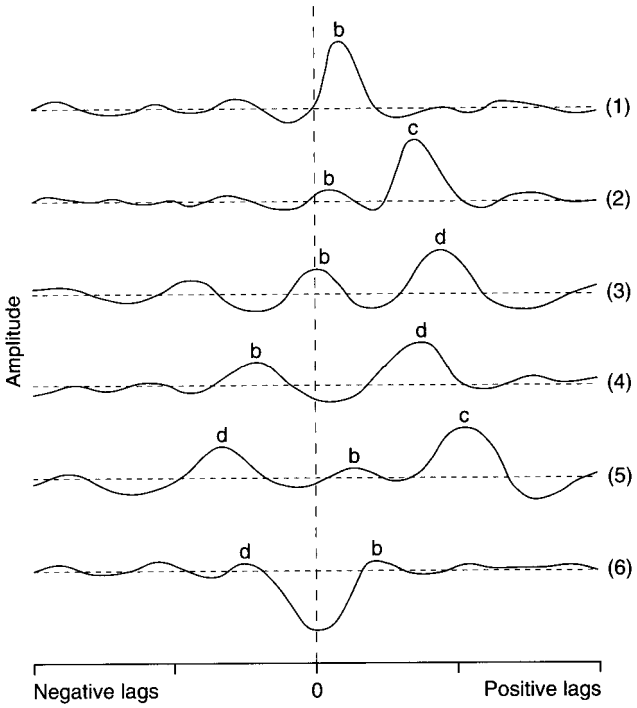

Figure 2.1.6- Diagram of possible time picks during cross-correlation. Peaks closest to time zero are labeled ***b,*** peaks greater than 10 dB above peaks ***b*** are labeled ***c***, and peaks labeled ***d*** are other possibilities. Trace 6 is a polarity reversal (after Cox, 1999).

not really exist; the problem lies in our inability to define the velocity field with the necessary accuracy and sufficient fidelity (Taner et al, 2007). Tomography emerged as a technique to define velocity cells with higher accuracy than conventional layer-based techniques by adding a second dimension, lateral variability, splitting the subsurface into cells instead of layers (Dines and Lytle, 1979; Bishop et al., 1985; Ivansson, 1985; Nolet, 1987; Wong et al., 1987; Stewart, 1991; Lo and Inderwiesen, 1994). For the tomographic technique raypaths from source to receiver are divided into segments and defined by cells. The objective of the method is to estimate the velocity, or slowness (1/V), of each individual cell by inverting first-arrival time picks (Figure 2.2.1) (Cox, 1999).

A model is produced from the first breaks on a shot record by minimizing the errors between the observed first arrivals and those computed by turning-ray theory (de Amorim et al, 1987). An initial model can be obtained via modeling or ray tracing using a single layer model with velocity increasing with depth

$$\frac{\partial V}{\partial z} > 0,$$

where V is velocity and z is depth. The output model is a product of the inverted initial model, and the differences between the modeled and observed times are updated during this process (Figure 2.2.2) by perturbing the velocities in the cells until the time differences are below a threshold set by the user (Cox, 1999).

The generalized linear inversion can be described explicitly by

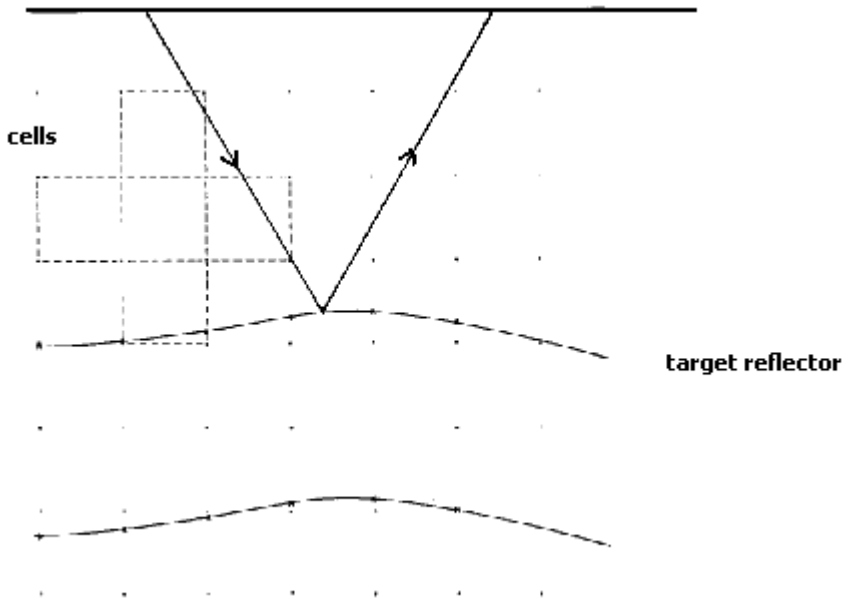

Figure 2.2.1- Diagram showing a reflection raypath intersecting cells in a tomographic image (modified from Bishop et al., 1985).

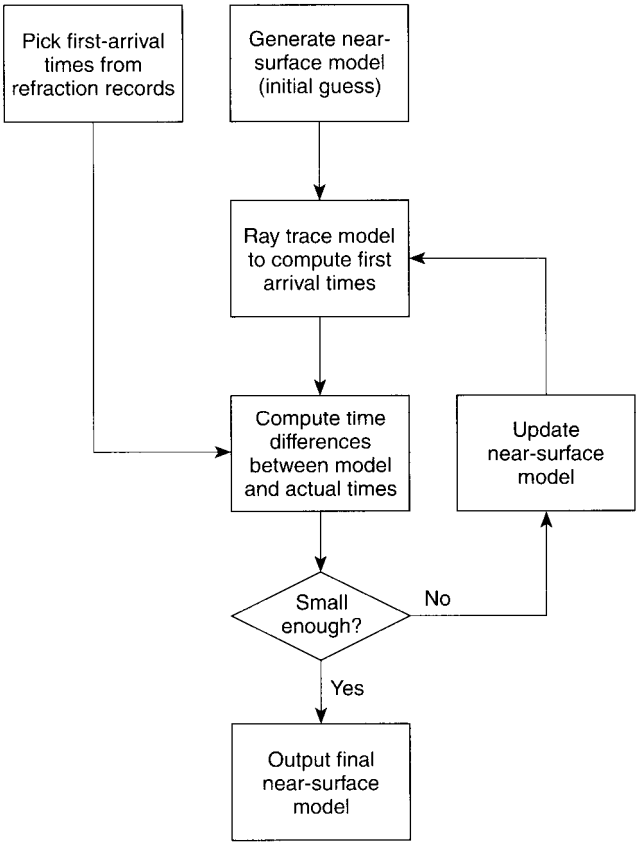

Figure 2.2.2- General inversion flow for a near-surface velocity image (after Cox, 1999).

$$Gm^{true} = d^{obs}$$

where **G** is an m x n matrix (m > n in both cases, m denotes the number of data and n the number of unknowns), and m^{true} and d^{obs} are the model and data vectors, respectively (Xia, 2009). There are limitations to the information that can be inferred from the refraction traveltime measurements, depth and slowness, even if they are exact (Bishop et al, 1985). Numerous algorithms exist to invert the generalized matrix, but some prevalent techniques are as follows: the algebraic reconstruction technique (ART), the simultaneous reconstruction technique (SIRT), the Gauss-Seidel method, singular value decomposition (SVD), and the Monte Carlo method (Cox, 1999).

In this highly non-linear problem (Nolet, 1987), when very little *a priori* information about the earth model is available, the instability and non-uniqueness are exacerbated and a regularized solution that minimizes data misfit is sought (Xia, 2009). Ideally, the difference between the calculated data and observed data is zero

$$d^{cal} - d^{obs} = 0$$

and a unique solution to the inverse problem would exist. In reality, however, because of model errors, errors in the observed data, and inaccuracies in the mathematical formulations, it is reasonable to look for a minimum rather than a zero value (Ivanov et al., 2005a).

$$d^{cal} - d^{obs} = \min$$

Minimization of the error *E(m),* from the method of least-squares, generates pseudo-solutions (Tikhonov and Arsenin, 1977),

$$E(m) = \left\| Gm^{est} - d^{obs} \right\|^2$$

(Figure 2.2.3), where local and global minima both exist (Menke, 1984). The absolute or global minimum is the best solution, however local minima complicate finding a solution to the inverse non-linear problem because they can be mistaken for the global minimum and create non-uniqueness (Ivanov et al., 2005a).

Smoothing is introduced as a regularization parameter, appended to the generalized inverse matrix (Ivanov et al., 2005a), that guides the solution using a moving average (Meju, 1994). The smoothing function attempts to capture important patterns in the data and show relatively slow changes of value while leaving out noise or small-scale structures. In tomography smoothing is represented by a parameter that is relative to the velocity, or slowness, gradient in the data. For instance, if there are sharp lateral changes in velocity, horizontal smoothing will average those changes making a particular cell a function of the values of the cells next to it. Smoothing decreases the tomographic resolution while helping minimize error during the inversion by increasing the number of rays that penetrate the sampled cells (Figure 2.2.4).

Dozens of tomographic solutions can exist for one set of first-break time picks because smoothing constraints are directly related to the variance (σ^2), or error, of the data (Menke, 1984). The practice is to pick a model according to the best combination of variance and resolution, however this is not necessarily the most

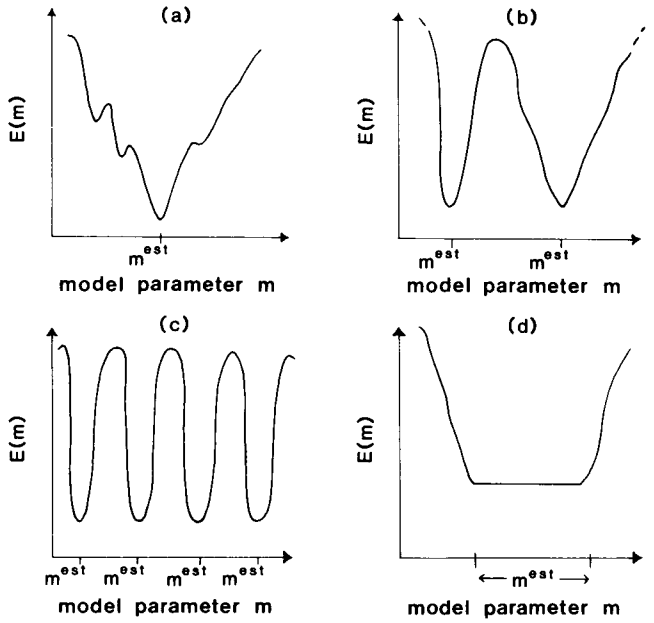

Figure 2.2.3- Diagram showing the severity of non-uniqueness during data inversion. There are four different examples relating the error function to a model parameter that show both local and global minima: (a) showing one unique solution and three local minima, (b) shows two solutions, (c) has many well-separated solutions, and finite range of solutions in (d) (after Menke, 1984).

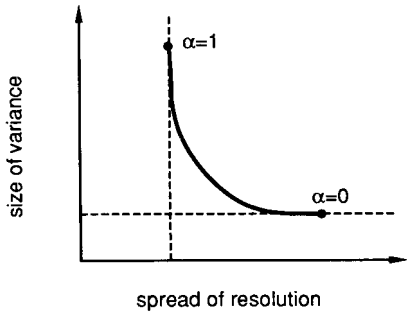

Figure 2.2.4- Traditional tradeoff between variance and resolution for a linear continuous inverse problem. Variance decreases with increasing spread of resolution (poorer resolution) because larger cell size minimizes error since it is an underdetermined problem. Regularization can also contribute to larger variance (after Menke, 1984).

representative of ground truth (Figure 2.2.4) (Menke, 1984). Non-uniqueness in geophysical inverse problems continues to be a controversial with no universal method of selecting the best model for application to the data.

2.3 Tomostatics

Turning-ray tomography has been shown to define the weathered zone with a high degree of accuracy both laterally and in depth (White, 1989; Simmons and Backus, 1992; Zhu et al., 1992; Stefani, 1993). Application of tomography to the statics problem, or tomostatics, is a natural evolution because of the reliability of an accurate near-surface velocity model (de Amorim et al., 1987; Zhu et al., 1992). The correction can be easily applied while correcting for topography. A main advantage to this approach is that the solution does not require layered refractors. Traditionally, static corrections are calculated vertically from the surface to a datum in the model, below which NMO velocities are more reliable because reflectors can be resolved in the shot gather (Zhu et al., 1992). Figure 2.3.1 and Figure 2.3.2 show the improvement from conventional datum statics corrections derived from a refraction survey when tomostatics is applied to the data (de Amorim et al.,1987).

The statics problem is notoriously time-consuming and ambiguous for any land seismic data with poor signal-to-noise (S/N) ratio, cycle skipping, truncated refractors, wavelets with indistinct first-arrivals, and topography (Taner et al., 2007). Historically, all effects that are time constant on seismic traces are considered “statics”, however it has been shown that abnormalities in the velocity and shape of the subsurface do not propagate through the wavefield evenly which brings to light

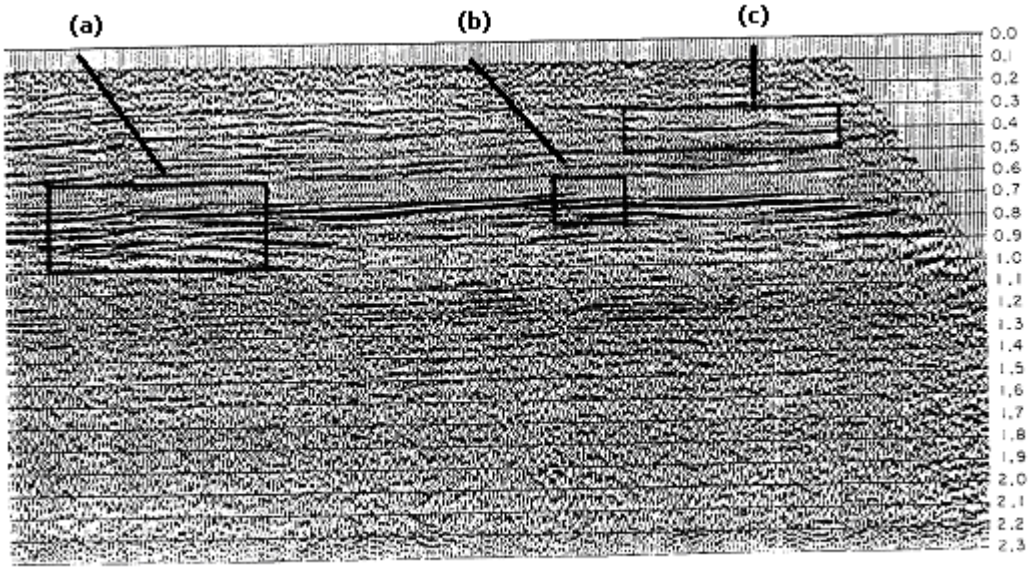

Figure 2.3.1- A CDP stack with conventional field statics (modified from de Amorim et al., 1987)

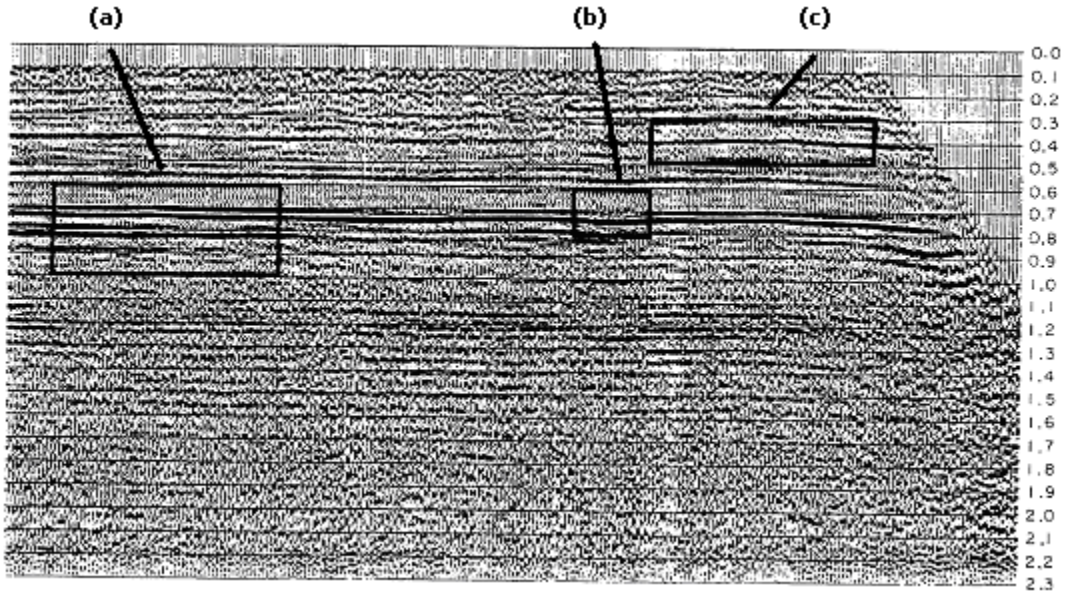

Figure 2.3.2- A CDP stack with tomostatics applied showing significantly improved reflection coherency at (a), (b), and (c) (modified from de Amorim et al., 1987)

"time-varying statics" (Taner, 1998; Taner et al., 2007; Berkhout and Verschuur, 2001). Near-surface research is especially sensitive to the displacement of raypaths through the low-velocity layer (LVL), hence there is a possible need for offset-dependent or angle-dependent statics corrections (Cox, 1999).

3. Procedure

3.1 Methodology for Angle-dependent Tomostatics

A new method has been developed in association with this research to address the geometry of reflection energy during tomostatic corrections, so that the correction is no longer vertical to the datum, but takes into account the raypath angle for a target reflector (Figure 3.1.1). This static correction will be based on a unique tomographic velocity-depth image created by inverting first-arrival time picks. Taking into account a prominent reflection, the static correction is calculated in the shot domain for the trace from each unique source and receiver pair following the relationship

$$V_{source} = \frac{\sum_{J} V_{nj}}{J} \qquad \text{and} \qquad V_{rec} = \frac{\sum_{J} V_{mj}}{J},$$

where V_{source} and V_{rec} are the average velocities over the J x K matrix representing the tomographic image (n corresponds to the raypath of the source and m the raypath of the receiver). The raypath length, d,

$$d = \sqrt{(J \cdot h)^2 + \left(\frac{x}{2}\right)^2}$$

where h is the cellsize and x is the source to receiver offset, allows the static correction

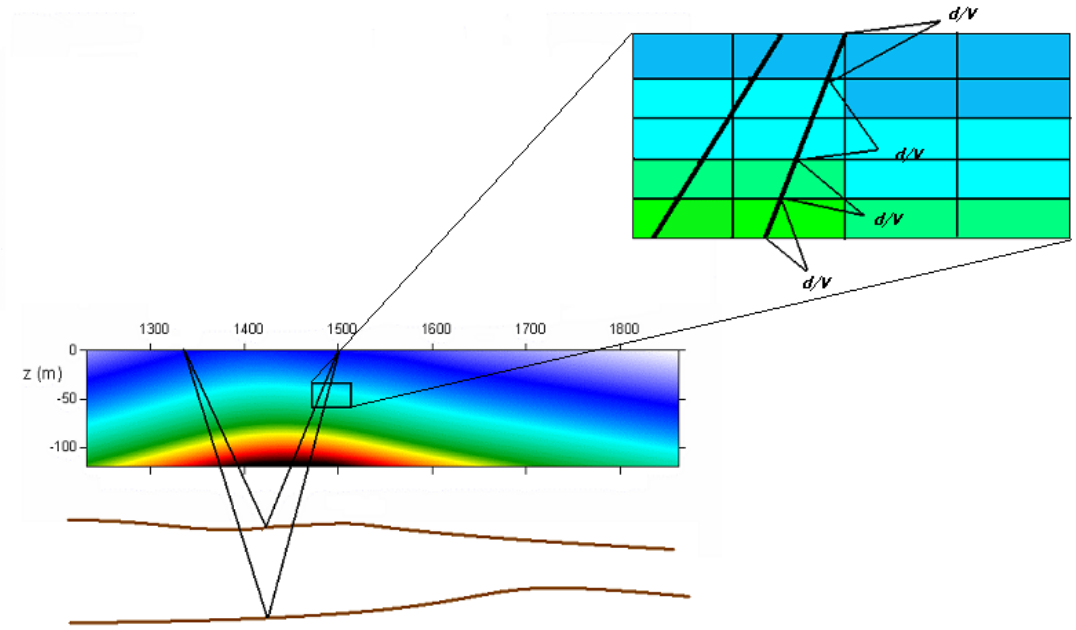

Figure 3.1.1- Diagram illustrating the angle-dependent tomostatic correction for the source and receiver of each trace. Both source and receiver raypaths are dependent on the target reflection.

$$t_{source} = \frac{d}{V_{source}} \qquad \text{and} \qquad t_{rec} = \frac{d}{V_{rec}}.$$

The time correction takes the target reflector into account using a ratio that is a function of the depth to the reflector, the NMO velocity, and the source to receiver offset. The depth to the reflector and NMO velocity can both be extracted from curve-fitting on a shot record, however this approach assumes flat-lying reflectors and is not always true. The source to receiver offset is taken from the trace headers in the data record and the tomostatic correction (in milliseconds) is, in turn, applied to the trace headers where an existing function in the processing software can implement shifting of each trace (Figure 1.1).

3.2 Reflection Correlation Coefficient (AUTS coefficient)

After tomostatics is applied, an assessment of the accuracy of the static correction must follow that relates to geology. Theoretically after NMO correction, the geology will emerge when the traces are horizontally stacked. The AUTS (Automatic Statics function in WinSeis Turbo) function measures trace-to-trace reflection coherency through surface-consistent statics corrections and creates a table of source and receiver corrections based on a target reflection in the data and a window in milliseconds. It also reports the number of failed correlations (Appendix A) based on the correlation coefficient threshold (0.1-1) set by the user. The number of bad correlations is directly associated with the reflection coherency. The AUTS coefficient is

$$AUTS = x \cdot n_f ,$$

where n_f is the number of failed correlations and x is the scaling factor. The scaling factor is used to dampen the large number of bad correlations if the correlation coefficient thershold is high, or the geology of the area is complex.

Assumptions associated with this AUTS coefficient are that the velocity function is accurate above that reflection and there is no significant faulting or folding that would interrupt reflection continuity. The AUTS coefficient is a tool used in two separate steps in this procedure: the first step is to choose a suitable initial model through smoothing tests and the second step is to monitor changes in reflection coherency as each iteration of tomostatics is applied to the data (Figure 1.1).

3.3 Smoothing Tests

Non-uniqueness exists for any inversion of geophysical data, so the ideal tomographic model is chosen using the angle-dependent tomostatic approach with AUTS to insure the best representation of the geology of the area. Tomography is run for 15-30 unique sets of smoothing constraints with the following parameters held constant:

1.) Initial Model (produced by tomography software from first-arrival picks)

2.) First-arrival picks

3.) Velocity boundaries

4.) Cell size

5.) Stopping RMS

6.) Allowed number of iterations

7.) Source locations

Angle-dependent tomostatics is applied to each model, followed by NMO correction, and AUTS targeting a relatively flat-lying strong reflection in the data. The tomographic model with the lowest AUTS coefficient represents the best solution for the target reflector window. It should be noted that automatic statics are not applied to the data at this point, the routine is simply used as a tool to assess which model is geologically viable. This is the first step before beginning iterative tomostatics and is only carried out to choose an initial model (Figure 1.1).

3.4 Iterative Tomostatics

Once the best model has been chosen through the AUTS coefficient, this number is considered the ambient reflection coherency and is compared to the AUTS coefficient after each iteration of tomostatics is applied (Figure 1.1). New first-arrival picks are made generating a new tomogram with this "best" model as the initial model. The tomography is damped according to the initial model, so that the solution will not deviate from what is considered geologically likely, and the smoothing constraints are kept constant through the iterations. The same process is repeated until the AUTS coefficient has decreased sufficiently. In the case that the AUTS coefficient does not decrease, either the initial model is the best possible solution for

the area or there is no global minimum (no best solution) due to the complexity of the geology or the data.

Conventional processing techniques follow iterative tomostatics, including residual statics to eliminate short-wavelength chatter and velocity analysis to account for changes affecting NMO. Coherency and geologic viability of the final stacked section will be compared to the original a stacked section produced using conventional processing.

The focus of this research is to include a fourth statics correction applied before application of surface-consistent statics to account for medium to long-wavelength statics, which takes into account reflector geometry via tomostatics. I propose using refraction tomography iteratively to define the LVL and correct reflection statics via angle-dependent tomostatics. This will improve reflection coherency in both shot gathers and the final stacked section while creating a geologically feasible velocity solution evidenced by surface-consistent correlation routines.

4. Synthetic Data

Testing of the angle-dependent tomostatic method requires removing any ambiguity resulting from non-uniqueness in the models introduced during tomographic inversion. An exact model of a near-surface setting and resulting wavefield can be obtained through full elastic forward modeling. Numerical seismic modeling using a finite-difference approach is widely used to generate synthetic seismic records from a defined discrete earth model (Zeng et al., 2009). To test the

angle-dependent tomostatic approach a finite-difference modeling program, developed at the Kansas Geological Survey by Chong Zeng, is used to create synthetic shot records with substantial static in the near-surface layer.

4.1 Finite-difference Modeling and Tomography

Tomostatics describes statics calculation generated from tomography. In this section the required static correction is calculated from the input model to the finite-difference program and therefore applied to synthetic data generated from the modeling routine. As an experiment to show the possible contrast in between "reality" (input model) and the calculated tomographic solution, a series of synthetic "shot gathers" were processed to simulate real data with first-arrivals that could be picked and inverted to produce a tomographic model (Figure 4.1.1, Figure 4.1.2, and Figure 4.1.3). Although this is only one possible solution, Figure 4.1.3 is a stark contrast to the constructed subsurface in Figure 4.1.1. The very near-surface (< 50 m) lacks detail laterally and therefore would not generate a thorough time correction. The apparent high velocity structures below 100 m are entirely false as well, even though there is significant ray penetration throughout the entire model. Further testing of the regularization parameter assignment is needed to effectively move to the next step and apply the tomographic component of this technique. The angle-dependent tomostatic algorithm must be tested using real "ground truth" input models.

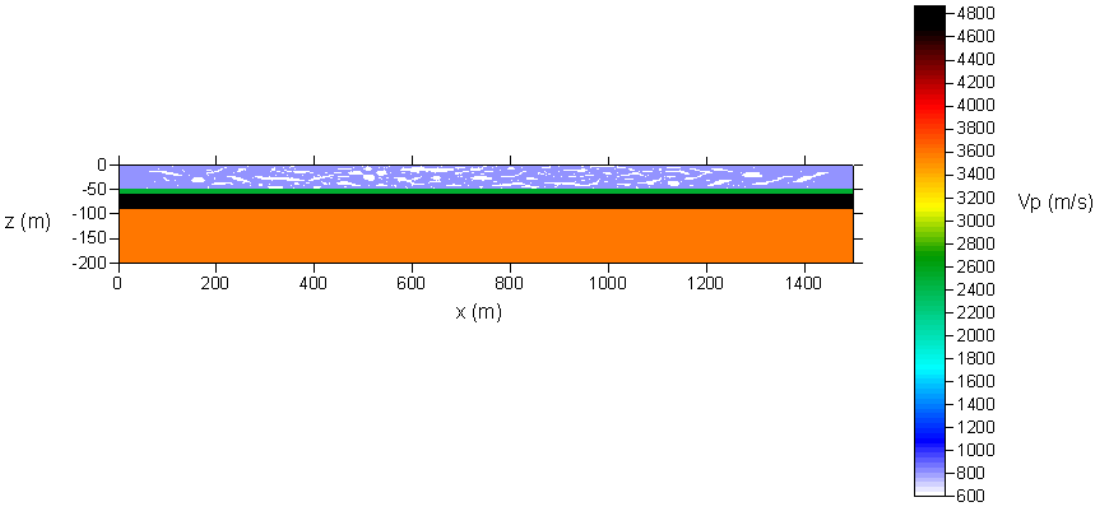

Figure 4.1.1- The input model for finite-difference forward modeling. This model was created using model-maker software specifically to maximize near-surface velocity variability.

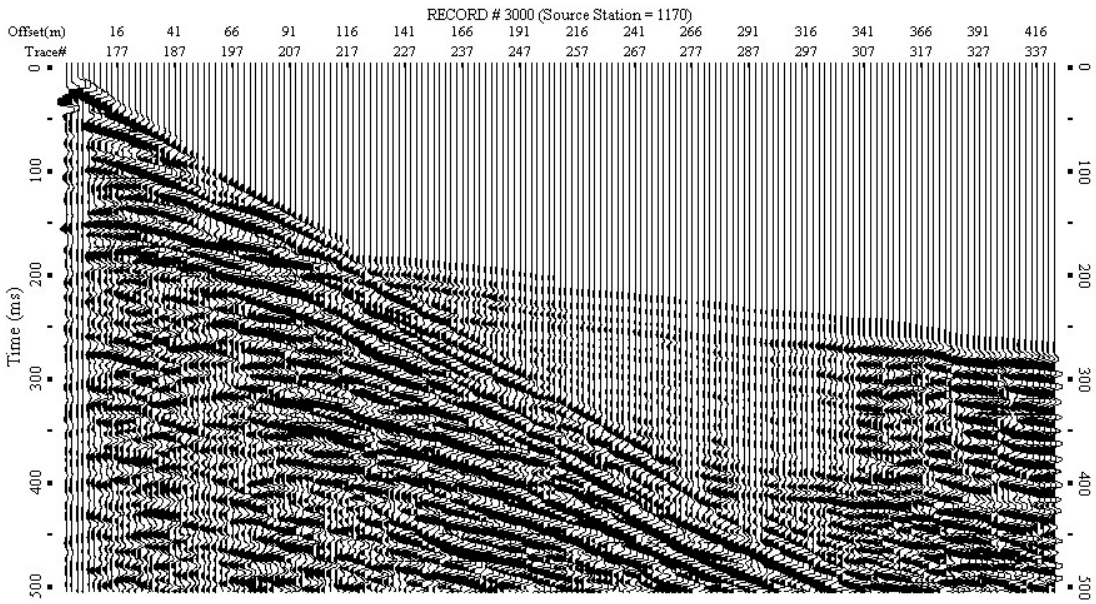

Figure 4.1.2- Synthetic data produced from modeling the wavefield propagation through model in Figure 4.1.1. First-arrivals were picked from 21 shot files.

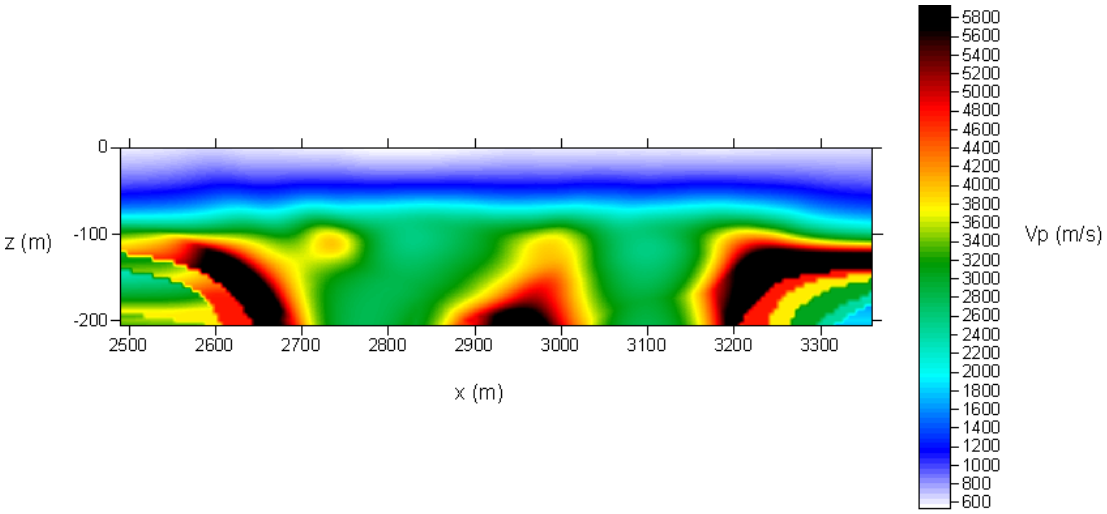

Figure 4.1.3- A tomographic solution to inverted first arrival picks from Figure 4.1.2 with a 2nd order smoothing of 1000 both horizontally and vertically.

4.2 Angle-dependent Tomostatics Using Finite-difference Modeling

The angle-dependent tomostatic method was developed based on the notion that near-surface velocity variability can cause short to medium-wavelength time shifts by perturbing the wavefront as it travels through a weathered medium that change as a function of angle of reflectance. A detailed velocity model for the near-surface with cells on the order of a trace spacing can be developed to locate velocity anomalies and account for them in a dynamic fashion on reflection seismic records by calculating the raypath of all shot and receiver pairs. The raypath is defined as the line perpendicular to the wavefront, which can be used to determine arrival time by ray tracing (Sheriff, 2002). Each shot receiver pair has a unique raypath for each reflection that diverges from the vertical assumption of conventional statics for very shallow reflectors such that if,

$$\tan^{-1}\left(\frac{x}{V_p t}\right) > 10^o,$$

where x is source to receiver offset, V_p is the compressional NMO velocity, and t is the two-way traveltime to the target reflector, the raypath no longer can be approximated as vertical. Many shallow seismic CMP studies have target reflections less than 30 m deep, and to maintain high S/N (large fold) a great range of offsets is needed, therefore, in many cases, the assumption of vertically incident rays is violated. The reflection angle, that is, the angle with respect to the normal of the reflection surface, should be taken into account to accurately correct shallow

reflections for time traveling through velocity variable material between reflector and receiver using the tomostatic method (Figure 4.2.1)(Sheriff, 2002).

A simple model was generated to emulate a geologic setting where travel time variability is observed from an anomaly less than a receiver spread in size, so-called medium-wavelength static (Pugin and Pullan, 2000). This model differs from the previous model (Figure 4.1.1) in that the synthetic data (Figure 4.1.2) generated from that model was too complicated for this evaluation. The model has 240 receivers at 2.5 m intervals and the seismic source at receiver station 60 on the surface. The source wavelet is a 60 Hz Ricker originating at the vacuum above the ground surface interface. To eradicate noise and confusion from the Rayleigh waves, air wave, and converted waves, the shear wave velocity (V_s) is 0. Attenuative boundaries are set at the left and right edges of the model to minimize boundary interference, and the bottom of the model is considered an infinite half-space (Virieux, 1986). The grid nodes are 0.25 m apart to a depth of 100 m, and the modeling time is 1 s at an interval of .0125 ms. The low velocity anomaly centered beneath station 124, 15 m in the z-direction and 30 m long, was created to resemble a sand lens (Figure 4.2.2).
The synthetic data record showing the effects of near-surface velocity variability is complex even with one subsurface anomaly, not only from a static time shifts perspective but also diffraction interference (Figure 4.2.3). The “clean” version of this data has no low velocity lens included (Figure 4.2.4). The Rayleigh resolution limit, ¼ λ, of a 60 Hz wavelet and 800 m/s velocity infers that objects greater than 12 m in the z-direction can be resolved, however if the object is laterally discontinuous,

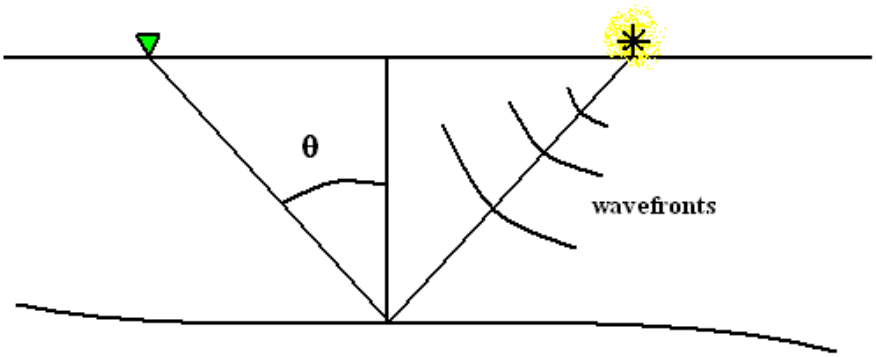

Figure 4.2.1- Diagram illustrating reflection angle with respect to the surface, where the shot and receiver are located. Wavefronts are radiating from the source and the raypath is defined as the line perpendicular to the wavefront (Sheriff, 2002).

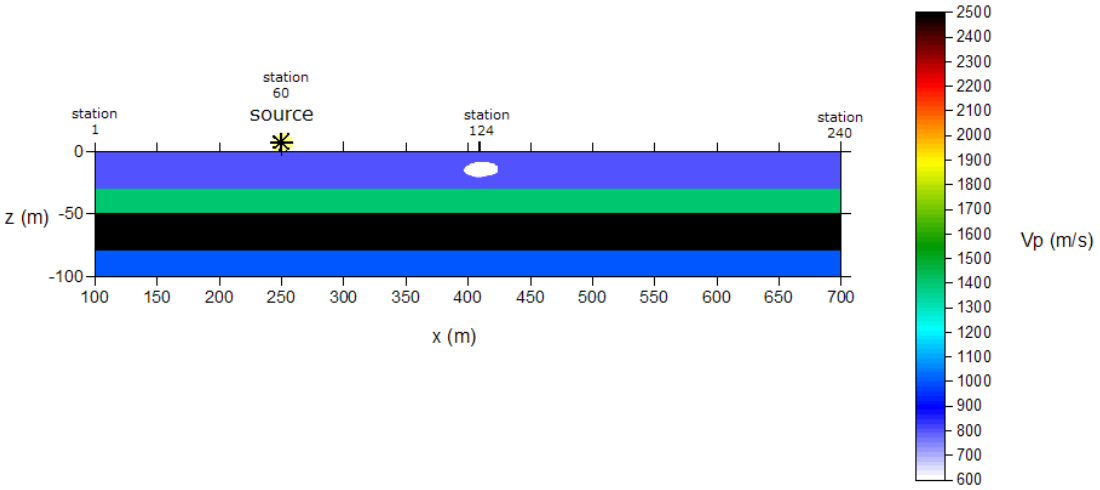

Figure 4.2.2 - Simple finite difference model with a near-surface velocity anomaly. The near-surface layer is Quaternary alluvium (shown in purple) with a velocity 800 m/s (ρ = 2.0 g/cm^3) with a low velocity anomaly material of 600 m/s (ρ = 2.1 g/cm^3). The near-surface layer overlies a 20 m thick shale-like layer (shown in green) with a velocity of 1400 m/s (ρ = 2.3 g/cm^3), a 30 m thick sandstone layer (shown in black) with a velocity of 2500 m/s (ρ = 2.54 g/cm^3), and a half-space (shown in blue) with velocity of 3000 m/s (ρ = 2.4 g/cm^3). Velocities modified from Carmichael (1989).

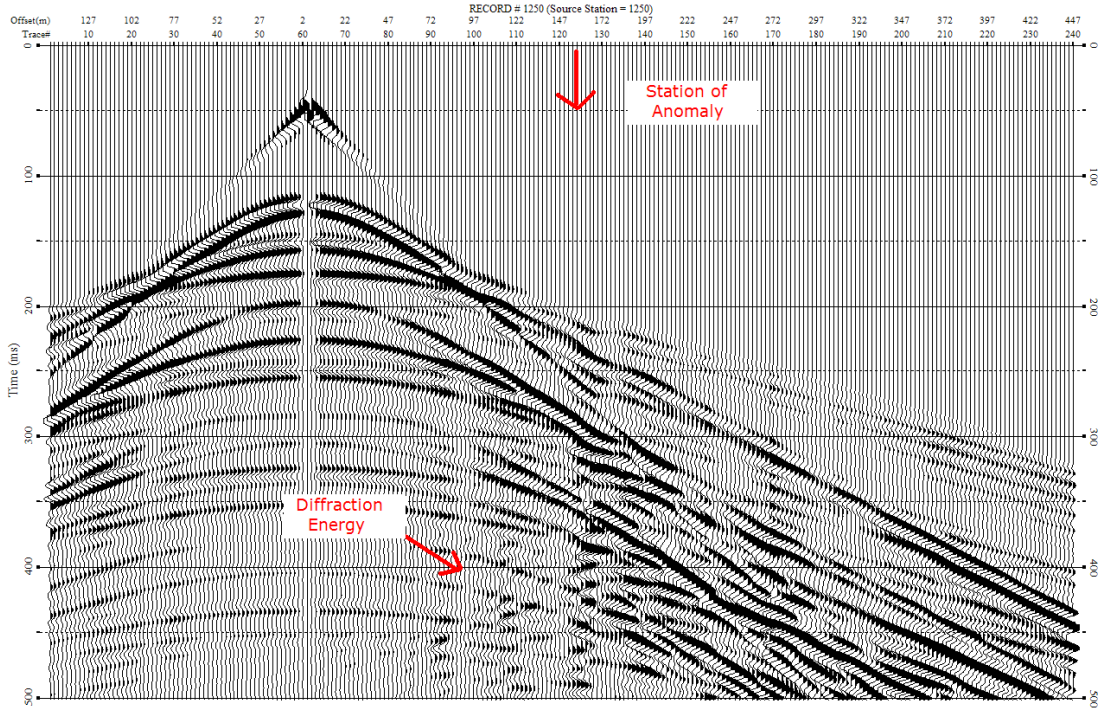

Figure 4.2.3 – Synthetic shot record from model in Figure 4.2.2, showing significant seismic interference due to medium-wavelength low velocity anomalies. Disruption of the first arrival energy and reflection energy can be seen near the station of the anomaly. Diffraction energy is traveling away from the anomaly location towards the left side of the record.

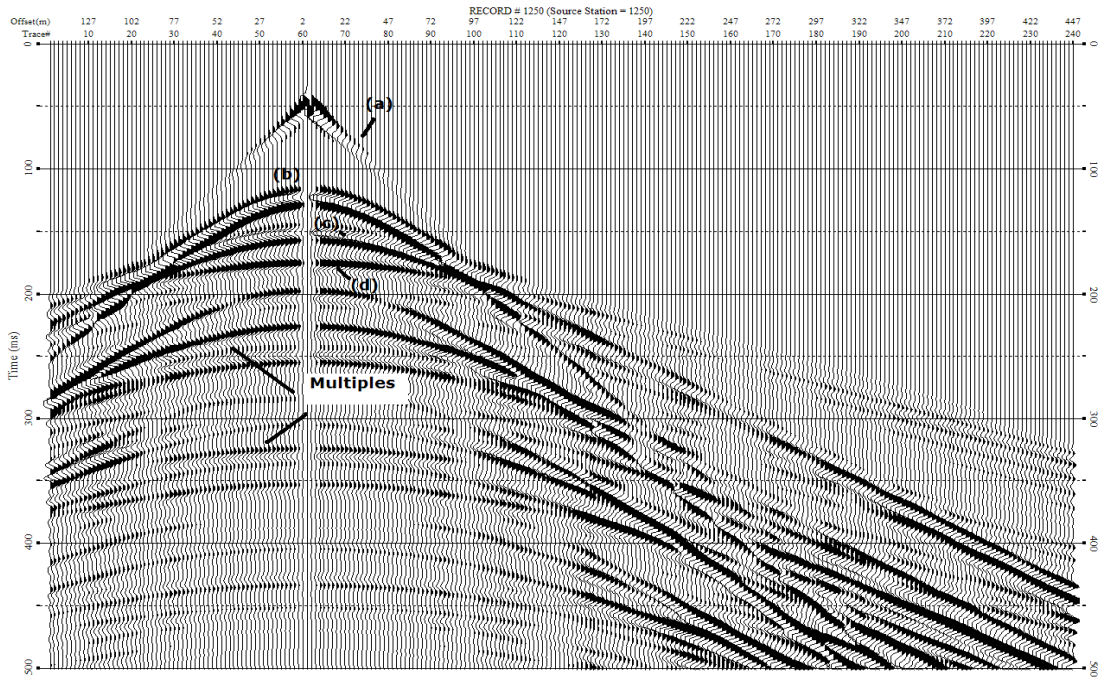

Figure 4.2.4- Synthetic shot record with no near-surface seimic anomalies seen in Figure 4.2.2. The record only contains compressional wave energy with the direct wave (a), the large amplitude reflection from the 800 m/s layer (b), the 1400 m/s layer (c), and the 2500 m/s high velocity layer (d). Significant multiple energy occurs below the first 3 reflections.

diffractions will be created at the edges (Sheriff, 2002). A diffraction is clearly visible in the data and is an excellent representation of the 3-dimensional nature of a perturbed wavefield (Figure 4.2.3). There are time delays near the station of the anomaly in the first-arrivals and reflections which continue through the multiple energy below 200 ms. This model represents an extremely simple case but one that should clearly test this approach to statics.

Angle-dependent tomostatics was tested on this dataset to a datum of 100 m. Average static time shifts[3] are 3-5 ms and difficult to see with low-frequency data, however with rigorous comparison using multiple visualization techniques a perceptible change is seen. Figure 4.2.5 shows the record after angle-dependent tomostatics has been applied with a target reflector of 175 ms and a velocity of 2500 m/s.

The angle-dependent tomostatic method tends to shift the data up as a function of offset, with a greater shift seen at longer offsets because of the longer path length through the model (Figure 4.2.1). This produces cycle-skipping in the data which in some places deteriorates reflection coherency so when the data is stacked it decreases the amplitude of the reflection (Figure 4.2.6). The angle-dependent algorithm takes into account actual source and receiver raypaths by approximating the velocities at the corner of the cell in the model using a ratio of depth of the reflector to offset, which allows the static corrections to be an integer value. These integer values increase at certain offsets as a function of the ratio, so while the correction does take

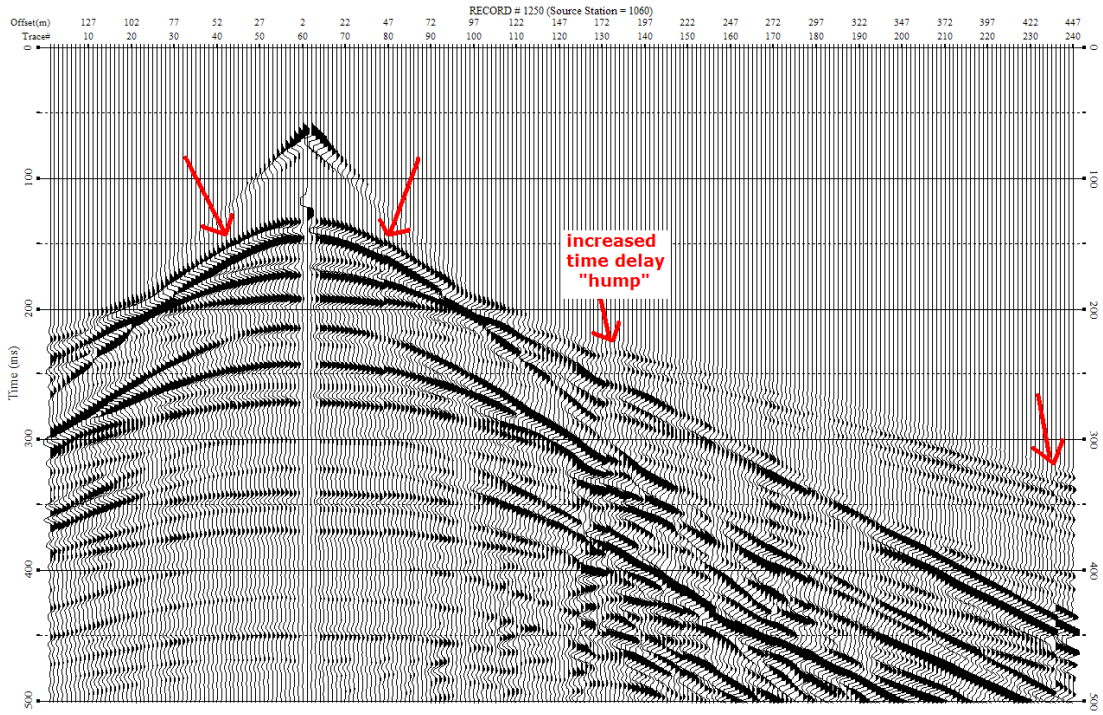

Figure 4.2.5- Synthetic record after angle-dependent tomostatics is applied. There are noticeable offset-dependent shifts on either side of the source as indicated by the arrows. There is also an increased static shift that creates a larger “hump” in the data near the station of the anomaly (also indicated by red arrows).

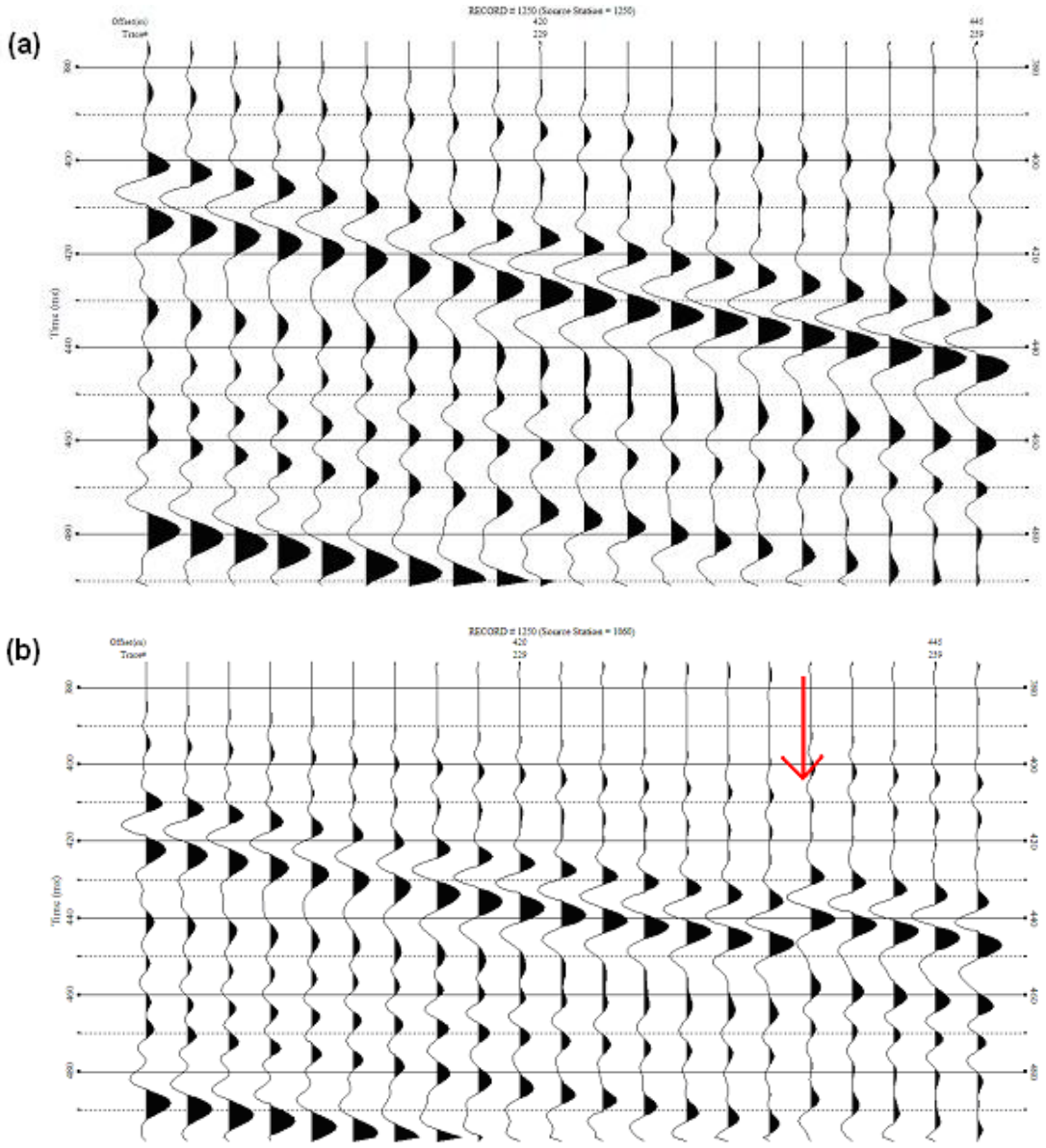

Figure 4.2.6- Synthetic data with angle-dependent tomostatics applied demonstrating decrease in reflection coherency due to offset (indicated by arrow). Data before angle-dependent tomostatics **(a)** and **(b)** after angle-dependent tomostatics is applied.

into account changes in velocity, there is a greater effect from offset. Also, small velocity changes are rounded out when converted to a time correction because it is an integer value, preventing high resolution, short-wavelength static corrections.

The traditional tomostatic methodology corrects the near-surface velocity variability vertically from the datum (Zhu et al., 1992), and has been routinely and repeteadly implemented in the past. Vertical tomsotatics will be tested using the finite-difference model to evaluate performance of the former angle-static approach. The extremely low-fold produced from one synthetic shot gather prevents useful measurements using the AUTS coefficient with these data. It will be helpful to explore the effectiveness of the AUTS coefficient and the proposed iterative approach to tomostatics when applied to real data.

4.3 Traditional Tomostatics Using Finite-difference Modeling

In this section the same approach will be used as above, except the velocities in the model will be vertically averaged for each source and receiver location without consideration for reflection angle (Figure 4.3.1). Therefore, this technique does not target any particular reflection in the data, only a datum within the model. Figure 4.3.2 shows the synthetic data with vertical tomostatic applied to a datum of 50 m. The average time shifts were from 3-5 ms and located at the stations affected by the low-velocity lense. The calculated static was a time delay (shift up) for all affected traces (112-136), however, there is an obvious time shift that remains

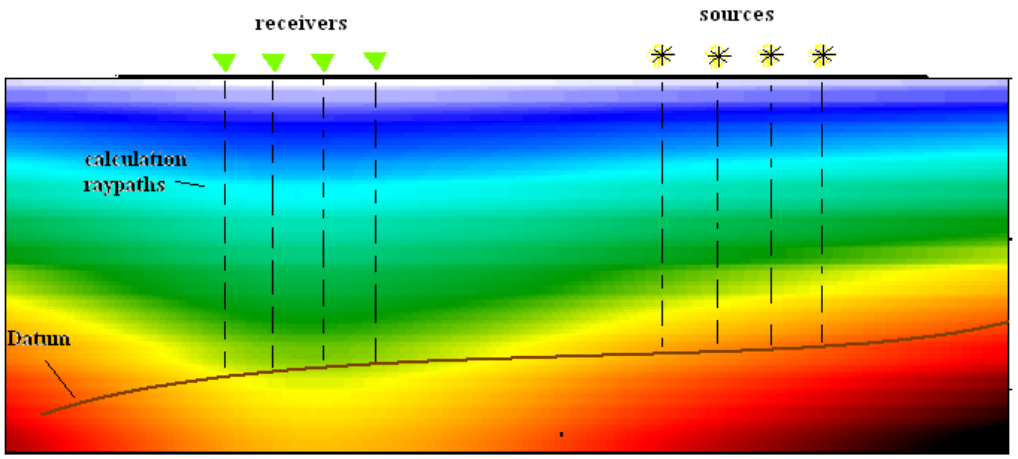

Figure 4.3.1- Diagram illustrating velocity calculation using the vertical raypath tomostatic approach.

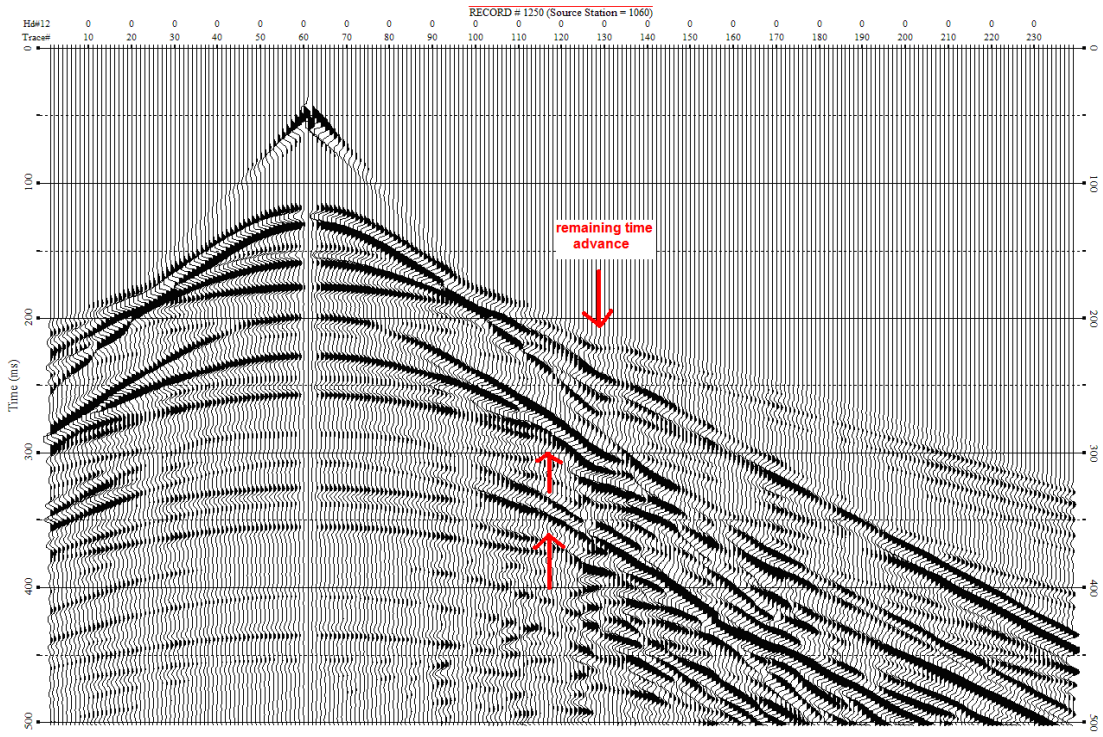

Figure 4.3.2 - Synthetic shot gather with vertical tomostatic applied to a datum of 50 m. The red arrows pointing up indicate a time shift implemented by the vertical tomostatics, however there are remaining time variations after in the data. One instance of remaining time advance is indicated.

uncorrected between traces 129 and 136. At this point in the subsurface the vertical length of the anomaly decreases and the full extent of the wavefield perturbation cannot be accounted for by vertical raypaths.

A change can be seen in the reflector coherency after vertical tomostatics is applied to these synthetic data (Figure 4.3.2). Although the increase in reflection coherency is very small in the shot domain, it may affect a stacked section appreciably because of improved trace alignment after NMO corrections. It is important to test this approach on real data that can be processed to a final stack in order to fully investigate viability of the proposed statics methodology.

4.4 Discussion

Angle-dependent tomostatics failed to show improvement in the shot gather domain, and in instances, this method actually damaged the stackability of reflections (Figure 4.2.6) for the simple model used to demonstrate the technique. The ineffectiveness of the angle-dependent tomostatic method is evident. The algorithm contains a large offset-dependence which decreases the resolution of the time correction, as well as its ability to detect lateral velocity variation. The AUTS coefficient routine was attempted on the data to test actual reflection coherency, but the low fold from the single synthetic shot gather inhibited the software from detecting any changes from either the angle-dependent or vertical tomostatics routines.

The vertical tomostatic approach uses purely velocity-based time corrections with depth to datum defining the length of the vertical raypath. The vertical

tomostatic approach better detects time variations due to velocity anomalies without degrading the reflection coherency, even when there are effects unaccounted for from velocity variablility in the near-surface (such as diffractions). The focus of the remaining portion of this study will be to test the proposed tomostatic approach on real data. This will be done by first identifying the best initial model by using the AUTS coefficient and monitoring progress through each iteration of the tomographic inversion on a chosen study area.

5. Hutchinson, KS

The static method, specifically the AUTS coefficient technique, was tested on data recorded near Hutchinson, KS targeting subsidence features. Field data contains high fold and a large range of offsets so that it may be processed using conventional techniques, specifically the statistical statics algorithms used to calculate the AUTS coefficient. These data offer a site with relatively flat, structurally unaltered stratigraphy away from the subsidence feature but extreme near-surface velocity variability in proximity to the sinkhole, which causes static issues.

5.1 Geologic Setting

A 2-D vibroseis survey was collected by the Kansas Geological Survey near Hutchinson, KS in collaboration with the Kansas Department of Transportation to investigate features in the subsurface that might threaten the U.S. Highway 50 bypass. The area has a history of major subsidence features due to salt dissolution and slumping of weathered overburden layers (Walters, 1978). Brittle deformation at the

surface causes severe lateral heterogeneity in the near-surface layers that can be detected by static shifts in seismic shot records.

The geology of the area is characterized by a sequence of shales, limestones, and dolomites of the Wellington Formation with the Hutchinson Salt Member located 270- 400 ft below ground surface at this site. The unconsolidated overburden is an approximated 60 ft. deep and consists of Quaternary gravel and sand deposits (Bayne, 1956). Subsidence is caused by leaching of the Hutchinson Salt Member, either by natural or man-induced dissolution processes, which results in a differential pressure between the overlying rock and the void space (Carter and Hansen, 1983). When the void space becomes large enough to exceed the strength of the roof rock brittle deformation occurs in the subsurface and continues up to the surface (Miller, 2006; Merriam and Mann, 1957). The unique contrast between the continuous, nearly flat-lying lithology (2-3% west dip) of the Permian carbonate deposits in the Wellington Formation and relatively flat topography, and the sporadic subsidence features across the area makes it ideal for a statics study solely due to the extreme near-surface velocity variability not related to topography or tectonic deformation of subsurface strata.

5.2 Seismic Acquisition and Processing

A continuous profile of reflection seismic data was acquired in 2003 along Highway 50 near Hutchinson, KS on the northeast edge of the extent of the Hutchinson Salt Member (Miller, 2006) (Figure 5.2.1). The survey was over 10 km long with 240 live channels per shot recorded with Twin Mark Products 40 Hz

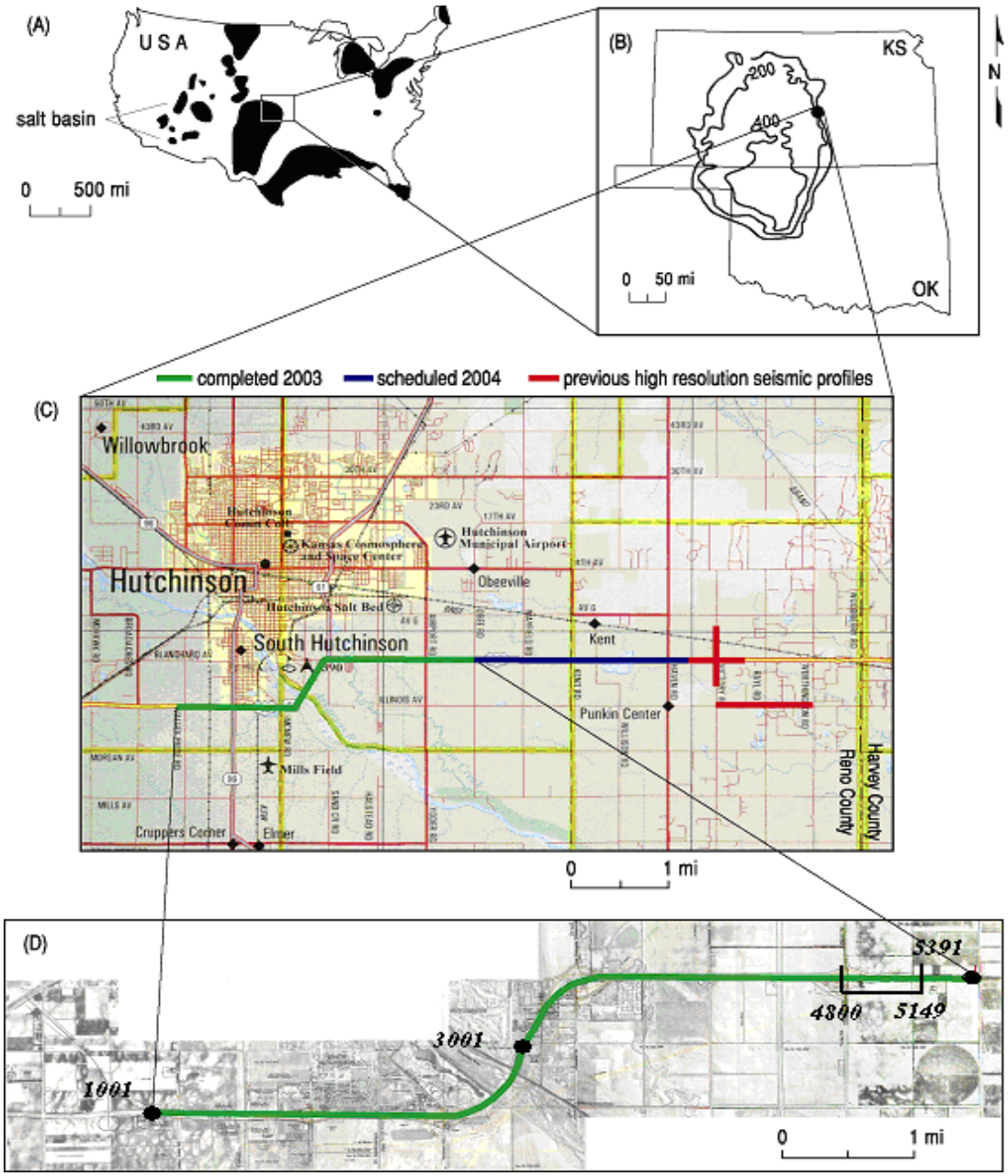

Figure 5.2.1- Survey site for seismic reflection in 2003 study along proposed U.S. 50 bypass. (A) Location of salt deposits in North America, with the northeast edge of the Hutchinson salt deposit highlighted in (B). (C) Highway 50 in relation to Hutchinson, KS and the completed seismic line along U.S. Highway 50(D) (After Miller, 2006).

geophones at 2.5 m intervals. Geophones were planted in firm soil at the base of a ditch along Highway 50 and four networked 60-channel Geometrics StrataView seismographs recorded data. The vibratory source was an IVI Minivib1 delivering three, 10-second, 25-300 Hz up-sweeps at shot stations located every 5 m along the receiver line. A fixed-rolling spread design was maintained throughout the 2-D seismic line (first 120 receivers were rolled to back of spread after shot 180).

The survey objective was to illuminate subsidence features that may threaten the stability of the road surface (Miller, 2006). The survey line was designed to provide a wide range of offsets with the dense spatial sampling necessary for detailed velocity analysis within the optimum window (Hunter et al., 1984) while maintaining a large spread for an increased imaging depth range. The section of data chosen for this statics research was between shot locations 4800-5149, located within the last quarter of the total profile. This section exhibited extreme trace-to-trace, near-offset static (2-6 ms) that was most likely due to the weathered layer because of the consistent nature of the time delays in those areas of the shot record, but different parts of the wavefield, as the source passed through (Figure 5.2.2). Since the static is caused by the weathered interval, the data can be used to test the AUTS coefficient routine using tomography to define this interval.

A common-midpoint (CMP) processing flow was used to process the data according to routine near-surface 2-D reflection methods (Steeples and Miller, 1990). Various software packages developed at the Kansas Geological Survey (WinSeis Turbo, SurfSeis, and TomSeis) were used to process and model the data. A

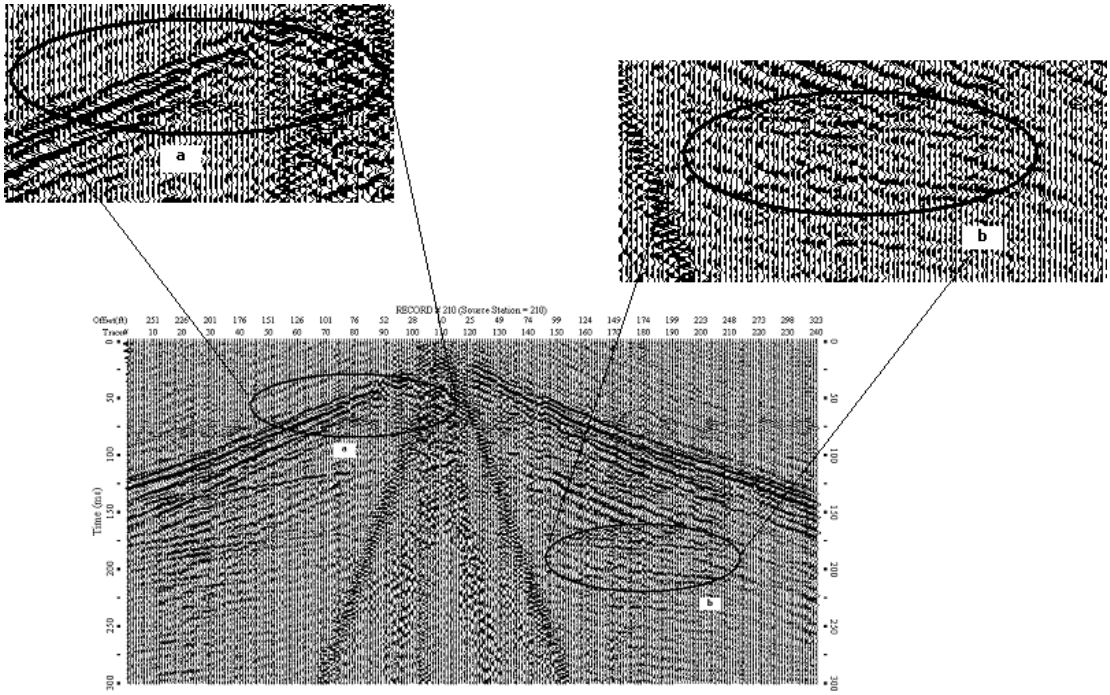

Figure 5.2.2-A shot gather showing significant static. The trace-to-trace time shifts shown in circle **(a)** are affecting the near-offset refractions and in circle **(b)** affecting two sets of reflections at 170 ms and 210 ms.

baseline processing run was completed using a conventional near-surface processing flow (Table 5.2.3). Raw vibroseis data were first pre-whitened and cross-correlated with a 25-300 Hz synthetic upsweep. Hardware settings in the field caused random shifting of the cross-correlated data, so a bulk static shift of 50 ms was applied pre-correlation. To minimize powerline noise, a hum filter was applied at 60, 120, and 180 Hz. Trace editing to remove noisy traces, airwave, and first-arrivals improved signal-to-noise and a low cut filter from 60 to 120 Hz was also applied. Datum statics were not applied to these data because the survey site did not have any topographic relief.

The data were processed (Table 5.2.3) to obtain a baseline AUTS coefficient before the smoothing tests were run (Figure 5.2.4). The AUTS routine was focused on a reflector at 232 ms and produced 7514 bad correlations out of 28,080 traces (Appendix A), resulting in an AUTS coefficient of 1502.8 (the scaling factor 'x' is 5). This is considered the ambient reflection coherency for the reflector at 232 ms (Figure 5.2.4), and will be compared to values extracted from tomographic solutions produced during smoothing tests to establish an optimal initial model for iterative tomostatics applied to these data in Hutchinson, KS.

5.3 Smoothing Tests on Hutchinson Data

The tomographic modeling software developed at the Kansas Geological Survey (Ivanov et al., 2005b) allows control of regularization or smoothing in both the vertical and horizontal dimensions, as well as the order of the smoothing (1st or 2nd derivative), and the stopping criteria (RMS error or number of iterations) (Figure

Table 5.2.3- Conventional CMP processing flow used for data. After datum statics **(A)**, there is an iterative process of automatic surface-consistent statics (AUTS) and velocity analysis **(B)**, followed by residual statics **(C)**.

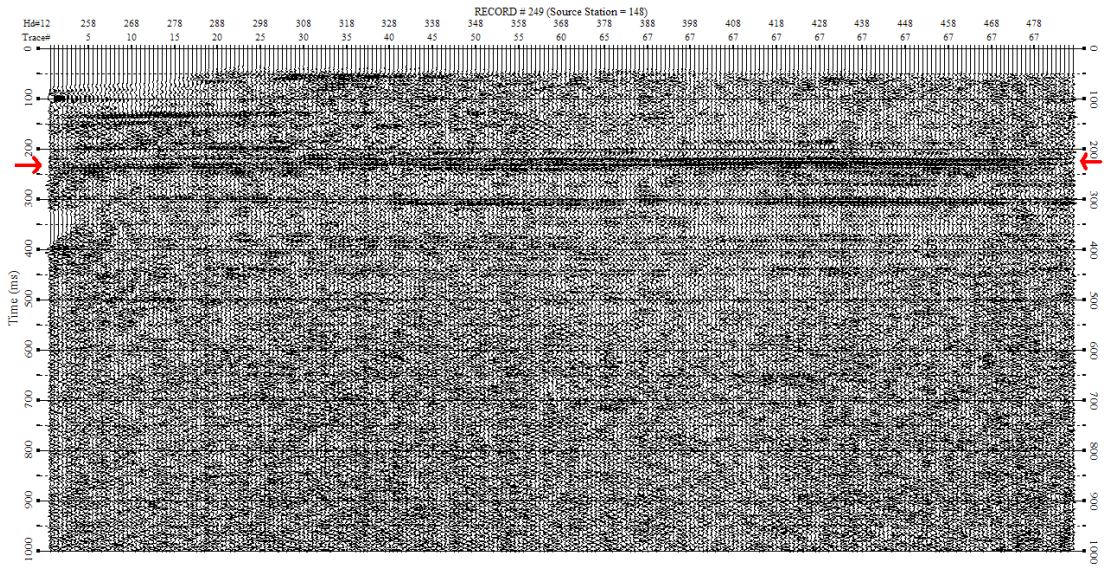

Figure 5.2.4- A stacked section of data from Hutchinson, KS processed using conventional techniques shown in Table 5.2.3. There is a strong reflection at 232 ms (see red arrow) which is the target window for the AUTS correlation.

5.3.1). Program input includes the following: first-arrival picks, source locations, boundary velocities, and any *a priori* information about the geology can be input through the initial model. In the event little or no *a priori* information exists, the program uses forward modeling to create an initial model from first-arrival picks (Figure 5.3.2). If the user creates an initial model, due to non-uniqueness, any model is an equally probable solution (Menke, 1984).

When solving linear problems, the simplest remedy for indeterminacy, or non-uniqueness, is smoothing. This approach, however, may produce a conservative estimate of the subsurface (Meju, 1994). In essence, the data is adjusted according to regularization constraints and thorough numerical testing is necessary to insure a reliable solution. Smoothing tests were performed on the Hutchinson data using the AUTS coefficient as a gauge for the best fit model. As mentioned above the stratigraphy is extremely flat and laterally continuous, so testing involved both combined horizontal and vertical smoothing and solely horizontal smoothing. First-arrivals were picked at 15 shot locations across the section of data and input for each tomography run. The stopping RMS was chosen to be around 2% of the longest first-arrival travel-time (~165 ms).

The processing flow for each tomographic model with unique smoothing parameters integrated the angle-dependent tomostatic approach (applied based on the 232 ms reflector) with an NMO-velocity curve of 2200 m/s and a datum at the bottom of the model (around 92.5 m). After this static was applied the traces were sorted into CDP's and NMO-corrected according to a standard velocity model. This step is

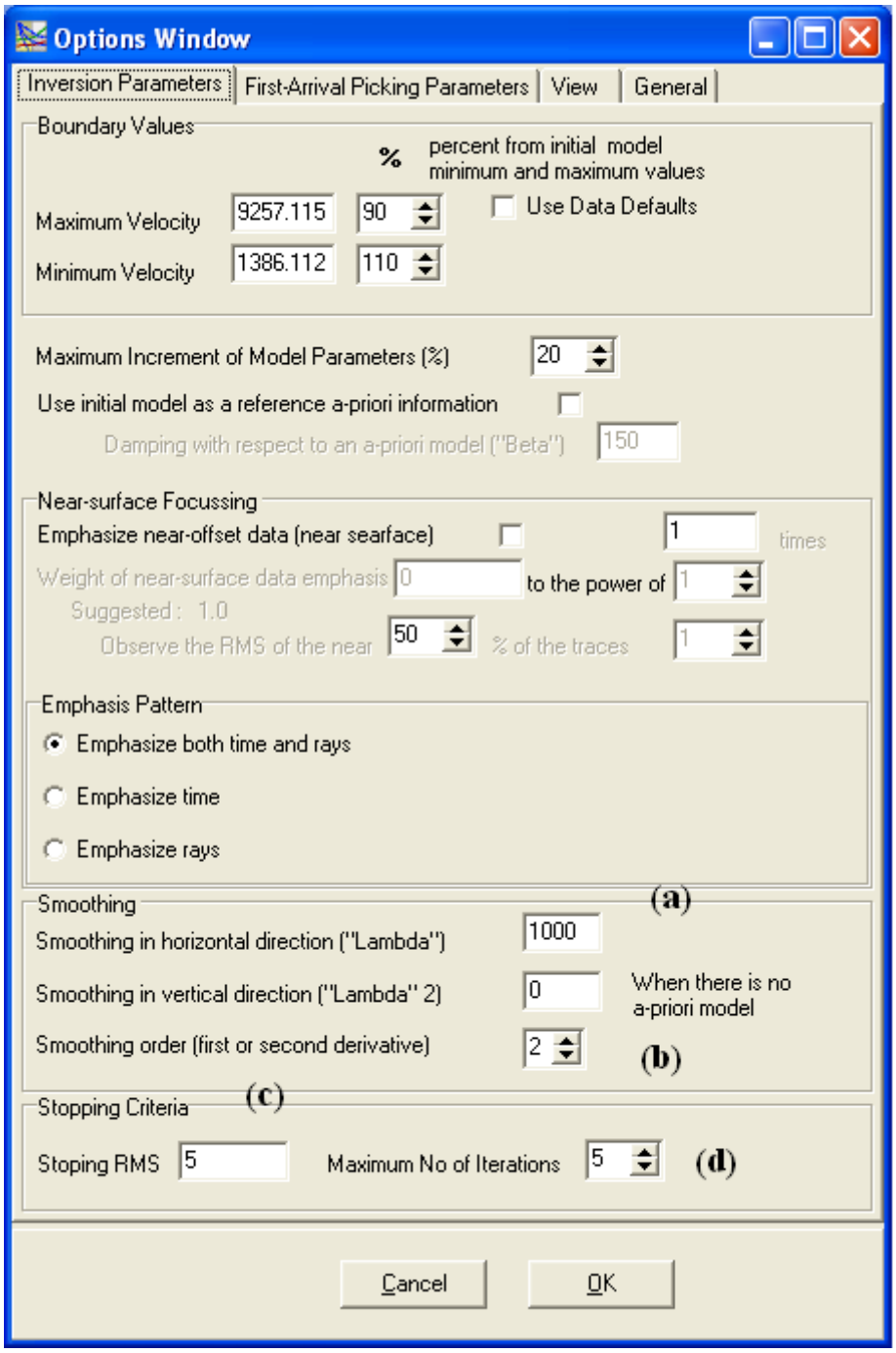

Figure 5.3.1- The graphical user interface (GUI) for the inversion parameters in the tomography software. Horizontal and vertical smoothing (a), and smoothing order (b) are pertinent to model creation. The program will stop iterating when it has either reached the stopping RMS (c), or the maximum number of iterations (d).

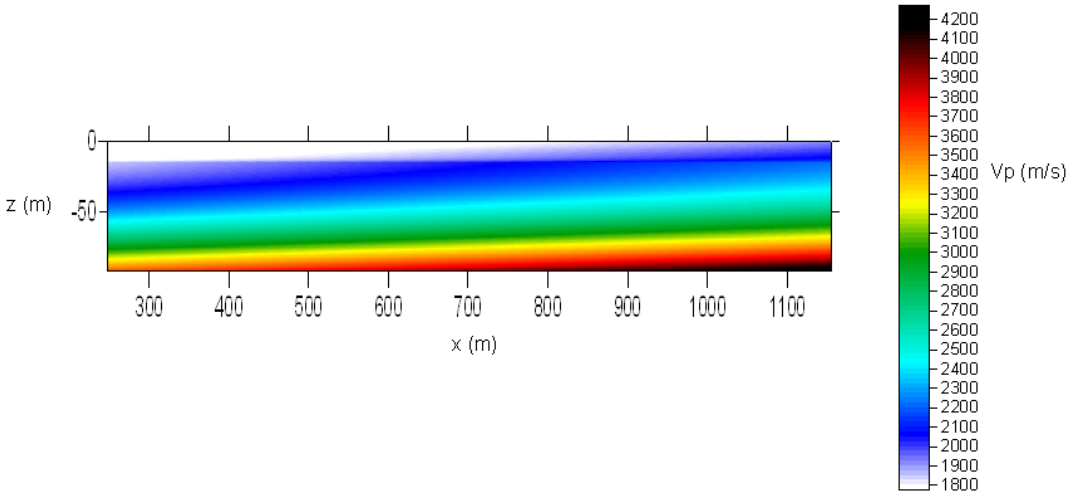

Figure 5.3.2- The initial model for smoothing tests, which was produced by forward modeling of the first arrival time picks. The boundary velocities were held constant with a minimum of 1347.02 m/s (85% of lowest initial velocity) and maximum of 4487.47 m/s (105% of highest initial velocity).

validated only because the static correction was less than 5 ms so it could be considered short-wavelength, and did not affect the overall velocity model (Hileman et al., 1968). Surface-consistent statics were then used to analyze the reflector at 232 ms while monitoring the number of failed correlations or the AUTS coefficient (Table 5.3.3).

Smoothing constraints ranged from 0 to 4500, vertically and horizontally, producing a total of 26 unique tomographic solutions for the input data. A smoothing constraint of 10 was used to represent 0 since a null value would be problematic for the algorithm. Furthermore, these number assignments are relative and only become clear through visual representation (Figures 5.3.4, 5.3.5, 5.3.6, 5.3.7). This tomographic solution to the first-arrival picks with virtually no smoothing applied, although patchy and geologically implausible, is mathematically possible, and cannot be discluded without *a priori* information or subsequent testing (Figure 5.3.4). Smoothing can have a dramatic effect on the solution and produce discrete layering or smooth structural changes (Figure 5.3.5 and 5.3.7). Either solution (1^{st} or 2^{nd} order) with a horizontal smoothing of 3500 is a possible representation of the geology near Hutchinson, KS because they both have laterally continuous layers. They each have unique characteristics as the 1^{st} order solution shows distinct layering (Figure 5.3.5) and the 2^{nd} order solution has a smooth velocity gradient (Figure 5.3.6). Smoothing both horizontally and vertically, however, completely changes the tomographic solution (Figure 5.3.7).

RMS (root-mean square) values associated with each model for the total

Smoothing				RMS (ms)			
Horizontal	Vertical	Order	# of iterations	Total	Near-offset	# of bad correlations	**AUTS** coefficient
10	10	1	2	2.34	2.06	8665	1733
10	10	2	3	2.99	2.26	10358	2071.6
1000		2	10	6.52	5.06		
1000		1	2	1.94	2.03	6746	1349.2
1500		1	4	2.23	2.2	6967	1393.4
1500		2	9	2.2	1.81	6944	1388.8
1000	1000	1	10	6.26	6.01		
1000	1000	2	1	1.86	2.3	7539	1507.8
2000		1	5	3.16	3.01	11478	2295.6
2000		2	10	7.68	5.58		
2000	2000	1	10	7.78	7.38		
2000	2000	2	1	2.1	1.95	7853	1570.6
2500		1	3	3	3.18	7229	1445.8
2500		2	1	3.85	2.19	7207	1441.4
3000		2	1	3.63	2.15	7057	1411.4
3000	3000	1	10	7.99	7.56		
3000	3000	2	1	2.06	2.05	7601	1520.2
3000		1	3	4.36	2.33	6838	1367.6
3500		1	3	1.98	2.05	6593	1318.6
3500		2	1	3.43	2.06	7006	1401.2
4000	4000	1	10	8.06	7.62		
4000	4000	2	1	2.1	2.16	7316	1463.2
4000		2	1	3.27	2	6829	1365.8
4000		1	3	3.14	2.6	6871	1374.2
4500		1	3	2.44	2.38	6725	1345
4500		2	1	3.13	1.95	6718	1343.6

Table 5.3.3- Table showing **AUTS** coefficient values (far right) for each set of smoothing parameters. Rows with no AUTS coefficients represent bad solutions to the picked first-arrivals with an RMS over 3.5 ms. If no vertical smoothing is shown, no vertical smoothing was applied during that test. The bolded box represents the lowest AUTS coefficient with a horizontal smoothing of 3500.

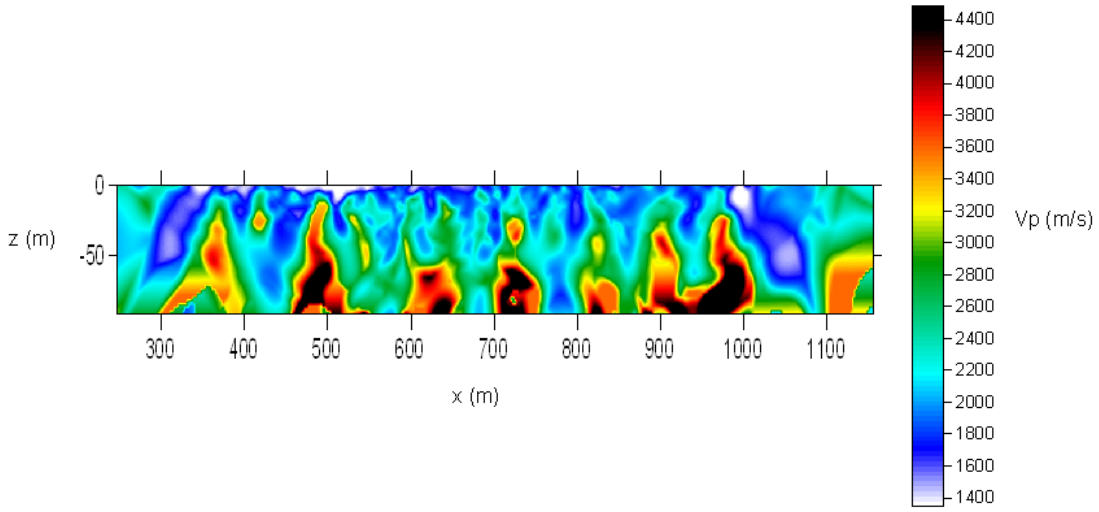

Figure 5.3.4- A tomographic solution with almost no smoothing applied; 10 both horizontally and vertically. The model is extremely erratic and demonstrates the unstable nature of this non-linear, underdetermined problem.

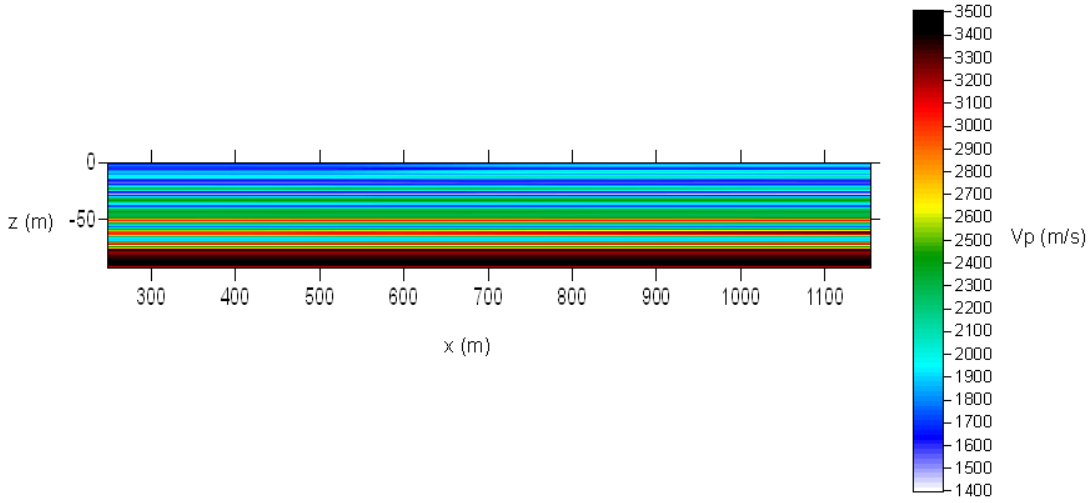

Figure 5.3.5- A tomographic solution with 1st order, 3500 horizontal smoothing applied. This model represents a laterally continuous, layered result.

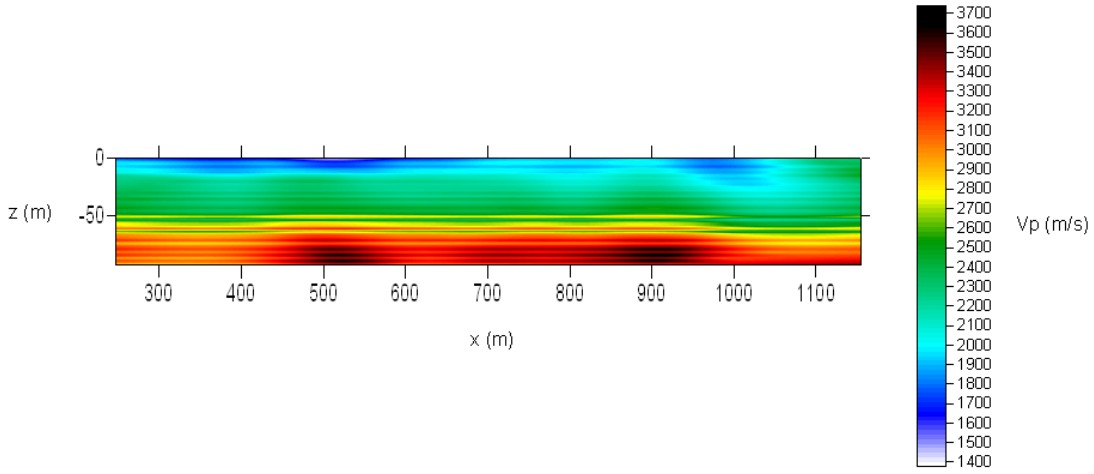

Figure 5.3.6- A tomographic solution with 2nd order, 3500 horizontal smoothing applied.

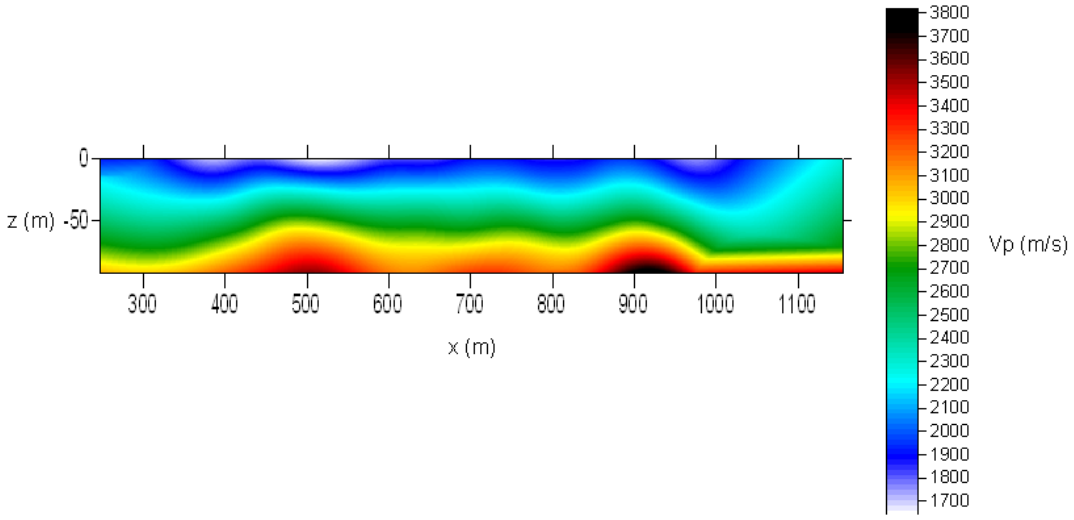

Figure 5.3.7- A tomographic solution with 2nd order, 2000 smoothing applied both horizontally and vertically.

solution and the near-offset time picks account for the variance in the mean of the final time measurements (Bevington and Robinson, 2003). RMS can be used to gauge the model accuracy, but does not imply precision or which model is physically more plausible. Once the tomographic RMS of the solution is below the set threshold, it is equally credible with all other solutions until tested. In this case, a correlation routine is used to establish the model that best corrects to a datum.

When smoothing was applied in both directions as a 1st order function, the ray coverage was lacking and the inversion did not converge on a solution, so the model was not considered (Figure 5.3.8). Overall, 1st order smoothing in the horizontal direction showed the lowest AUTS coefficient. These models tend to have discrete, uniform layers with sharp transitions between layers and lateral homogeneity (Figure 5.3.5). The extremely smooth solutions (2nd order smoothing in both directions) have gently dipping structures and uniform velocity gradients (Figure 5.3.7) and also have the highest AUTS coefficient (Figure 5.3.8). These solutions do not improve reflection coherency in the stacked section. The solution with the overall lowest AUTS coefficient from this specific set of first arrivals was a model with 1st order horizontal smoothing of 3500 (Figure 5.3.5). This model will be considered the best initial model for the geology of the area.

5.4 Angle-dependent vs. Vertical Tomostatics

The angle-dependent tomostatic approach was tested on synthetic data (Section 4.2) and compared to the vertical tomostatic approach (Section 4.3), which showed that there are some limitations in the angle-dependent algorithm that cause a

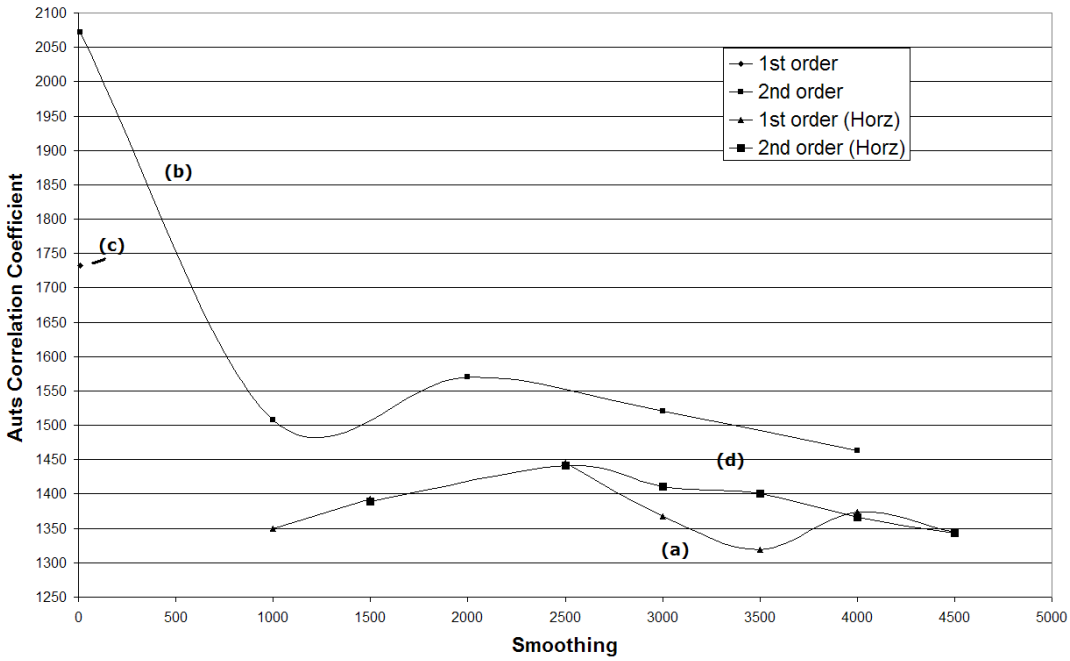

Figure 5.3.8- Results from smoothing test on Hutchinson, KS data with trends for each type of smoothing. **(a)** The overall lowest **AUTS** coefficient was 1st order horizontal smoothing, and **(b)** the overall highest **AUTS** coefficient with 2nd order smoothing in both directions. **(c)** 1st order smoothing in both directions only had one viable solution with a smoothing of 10, and **(d)** represents the 2nd order horizontal smoothing solutions.

deterioration of the reflections. Both methods were tested on field data where the AUTS coefficient could be used to monitor progress through the iterations. During processing of each approach, tomostatic was applied to the best initial model chosen from the smoothing tests, 1st order smoothing of 3500 (Figure 5.3.5), followed by an NMO correction and AUTS.

Application of angle-dependent tomostatics to data collected near Hutchinson, KS produced the same inaccuracy in the shot domain that was seen in the synthetic data tests: cycle-skipping. (Figure 5.4.1). The AUTS coefficient after tomostatic correction was determined to be 1318.6, which is an improvement from the baseline coefficient of 1502.8. Any method for correcting statics should not cause discontinuity in the reflections in the shot domain, so the angle-dependent approach will not be implemented iteratively on the Hutchinson data.

Vertical tomostatics was tested on the data with a datum of 50 m, which was determined by numerical analysis of three datums: 92.5 m, 50 m, and 30 m. The first

iteration of tomostatics showed an improvement in the AUTS coefficient over both the baseline AUTS coefficient and the angle-dependent tomostatic method (Figure 5.4.2). The second iteration of tomostatics also improved the reflection coherency as seen from the AUTS routine, however the third iteration had an increase in the AUTS coefficient. This could be indicative of two possible outcomes: either the best tomographic model is reached after two iterations, or more iterations are needed to optimize the model. To test this, another iteration of vertical tomostatics

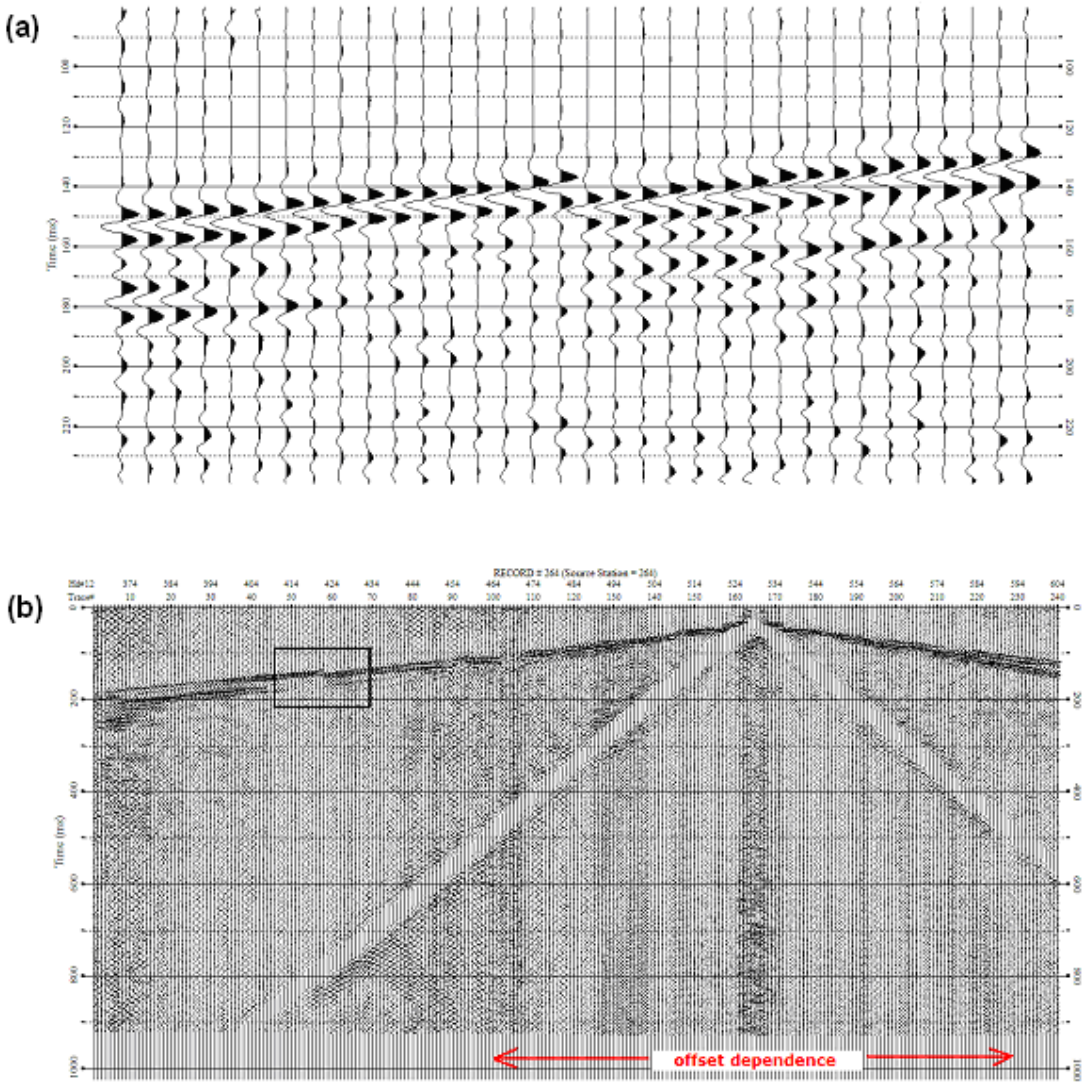

Figure 5.4.1- (a) Example of cycle-skipping from angle-dependent tomostatic method applied to the Hutchinson data. **(b)** Shot gather showing offset-dependence that can be seen as a greater time shift for traces with increasing distance from the source. **(a)** is the enlarged box from **(b)**.

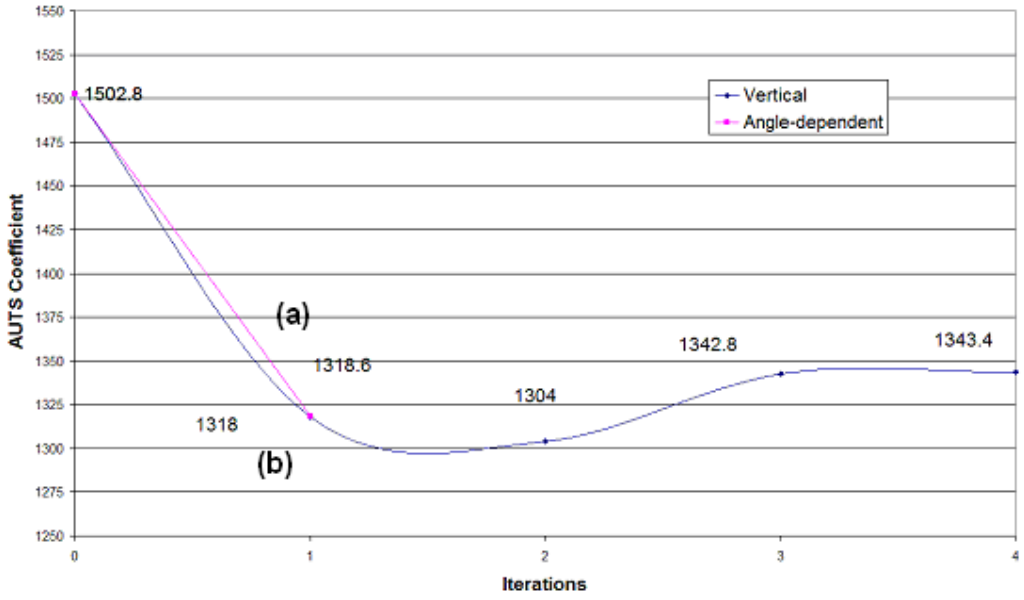

Figure 5.4.2- Results from angle-dependent and vertical tomostatic application on the Hutchinson data. The AUTS coefficient is the weighted number of bad correlations from the cross-correlation function. Angle-dependent tomostatics showed a decrease in AUTS coefficient, **(a)**, but vertical tomostatics, **(b)**, produced a greater increase from the same baseline value.

was applied to the data and the AUTS coefficient continued to increase (Figure 5.4.2). This trend is interpreted to indicate that the tomostatic correction is optimized on the second iteration (Figure 5.4.3).

5.5 Discussion

The smoothing tests indicated that a specific type of regularization produces the seismic image that best matches the geology in the Hutchinson area. Model velocities in the upper 25 m range from 1400 m/s to 2000 m/s in the model, likely corresponding to the unconsolidated material reported to be between 20 and 25 m (Bayne, 1956). There is a notable transition between approximately 25 m and 80 m to velocities ranging from 1800- 2500 m/s. The Upper Wellington Shales correlate to these depths (Miller, 2006) with reported velocities consistent with the model. The model can be extended to a depth of almost 100 m where velocities as high as 3500 m/s are estimated, but cannot be associated with true geology below that due to lack of ray coverage (Figure 5.4.4).

The smoothing tests produced a geologically realistic initial model that was used as the first iteration of tomography to test angle-dependent against the vertical tomostatic approach. The angle-dependent approach created the cycle-skipping that decreases the continuity of reflections in the shot domain, however, it also had a decrease in the AUTS coefficient. This is counter-intuitive but a possible explanation could be that the 8-9 second shifts causing the cycle-skipping may not have a large affect on NMO-corrected data because both are a function of offset. This, however, cannot be verified without further investigation. Vertical tomostatics showed a

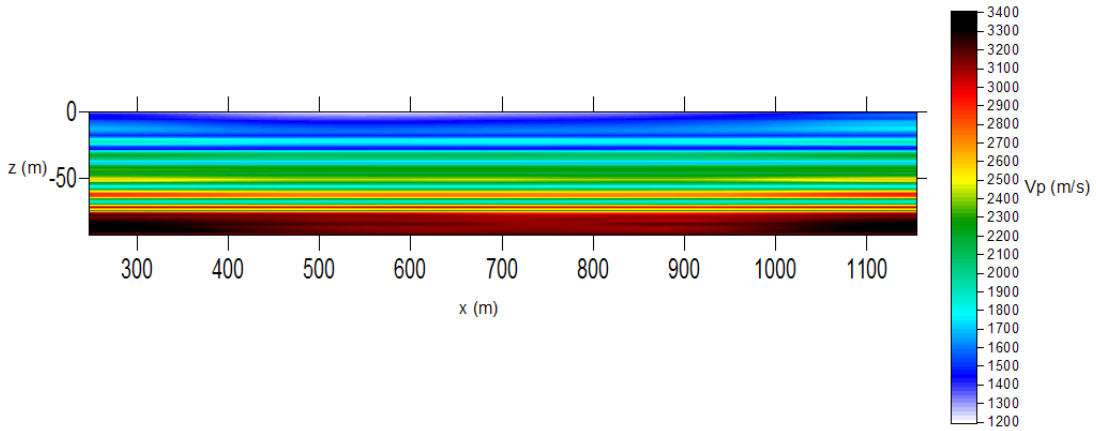

Figure 5.4.3- The tomographic solution on the second iteration of tomostatics applied to Hutchinson data.

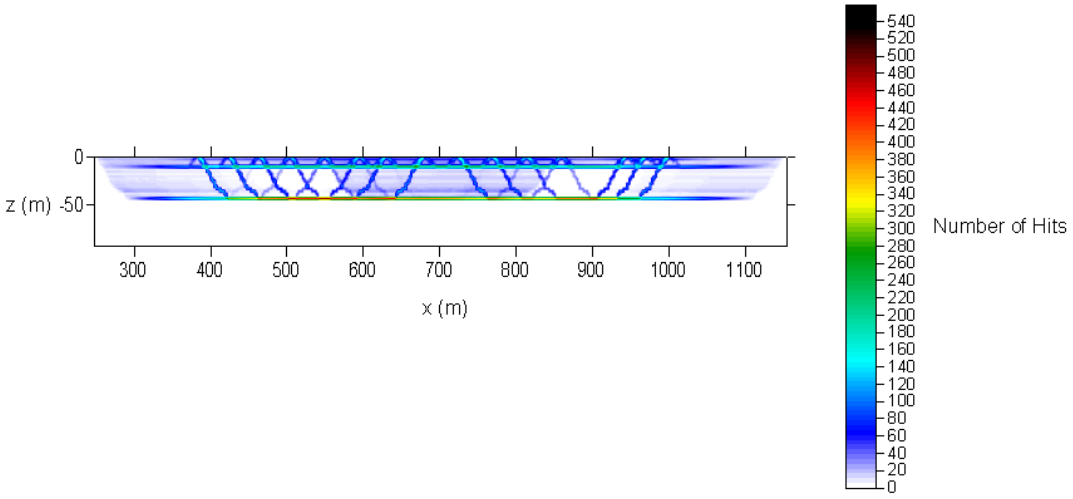

Figure 5.4.4- Ray coverage diagram for model in Figure 3.4.6. The color corresponds to number of hits in that cell, and only reaches 50 m or 164 ft.

greater improvement in the AUTS coefficient on the first iteration, which decreased further on the second. The third and fourth iterations deteriorated reflection coherency, indicating an optimized model on the second iteration that was similar to the initial geologic model (Figure 5.4.3). The final stack after iterative vertical tomstatics, showed an increased reflection coherency in some areas (Figure 5.5.1).

6. Twin Creeks, NV

Reflection seismic data was collected in the high desert of Nevada to study different approaches for enhancing near-surface seismic reflection data to allow improved delineation of structures that are consistent with the occurrence of gold-bearing sills in this area. This highly weathered mature topography (Figure 6.1) causes seismic energy arrival variability or "statics" representing a significant problem. The surface geology at this site does not reflect the presence of the highly variable weathered and subweathered strata that are a result of colluvial infill and compaction over the structurally altered bedrock (Cox, 1999). Horizontal layering, homogonous velocities, and uniform depth-to-bedrock are very unlikely in this region, making it extremely difficult to produce CMP reflection sections that accurately represent the subsurface geology at a useable S/N. An iterative vertical tomostatic approach that optimizes the near-surface tomographic velocity model using AUTS will provide the appropriate level of guidance to improve near-surface reflections in this data.

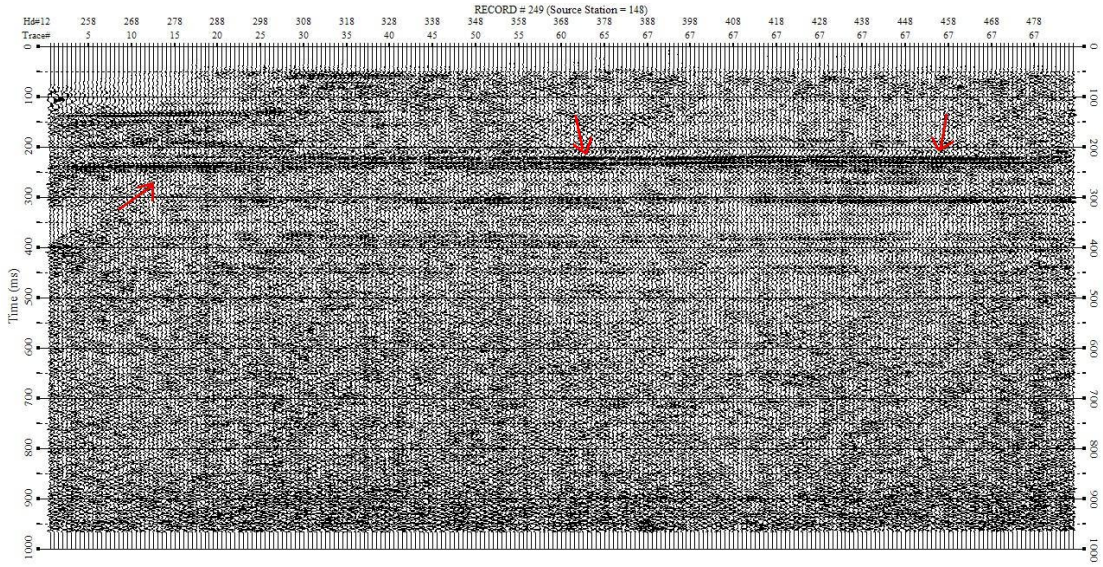

Figure 5.5.1- Final stacked section of Hutchinson data after 3 iterations of vertical tomostatics. Places of improved appearance of reflection coherency indicated by arrows.

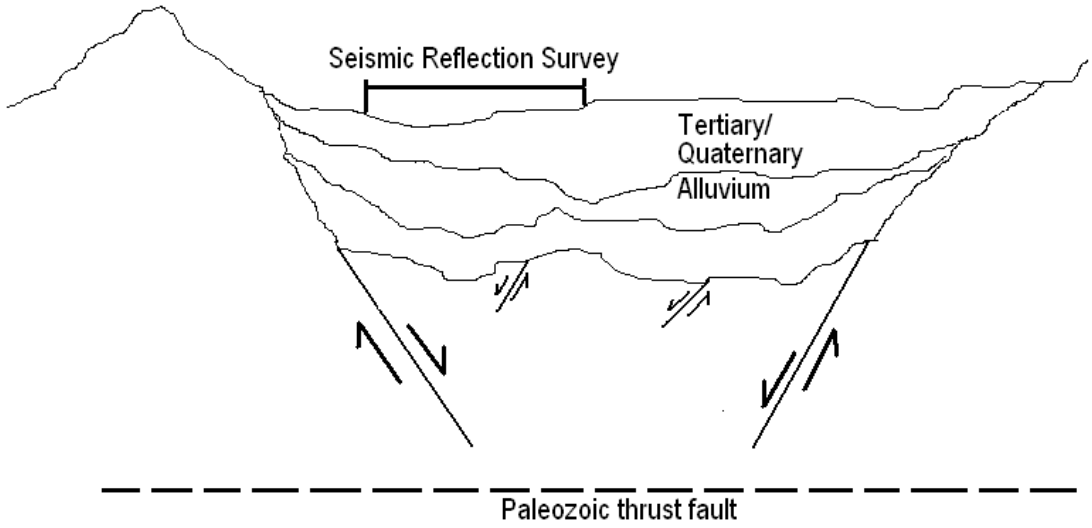

Figure 6.1- A conceptual diagram of mature topography with complex structural deformation in the basin and range (not to scale).

6.1 Geologic Setting

A high-resolution 2-D reflection survey was conducted two miles south of Twin Creeks Mine in Humboldt County, NV. This survey is meant to highlight structures with local resource potential and sample an area with extreme statics issues (Figure 6.1.1). The project, sponsored by Newmont Mining Corporation, targets the Paleozoic sedimentary rocks containing disseminated gold deposits. Significant statics problems represent a major obstacle and must be addressed to produce an accurate time representation of the geology. The geology of the area is dominated by both low- and high-angle faults and folds associated with the Golconda and Roberts Mountians thrust (Breit et al., 2007). The high-angle faults in the area mostly strike north-south and are cut by Quaternary alluvial fan deposits (Figure 6.1.2). The area is highly mineralized in association with sills and dikes intruding through structurally altered Paleozoic sedimentary and igneous rocks. Gold-bearing quartz veins and hydrothermally altered carbonates are the principle hosts targeted by most exploration efforts in the area. These features are routinely associated with structural highs such as anticlines or uplifted fault blocks.

The mine is located in a broad valley with 0-250 m (800 ft) of Quaternary alluvium that has been deposited along the northwest trending Dry Hills Range. The alluvium contains clasts of basalt, limestone, and hematitic clay (Breit et al., 2007). The reflection survey line is located ~2 miles south of the Twin Creeks MegaPit[4] (Figure 6.1.2), so, the geology should closely relate to that shown in the B-B' cross-

[4] A MegaPit is a large open-pit mine used to extract materials when they are close to the surface.

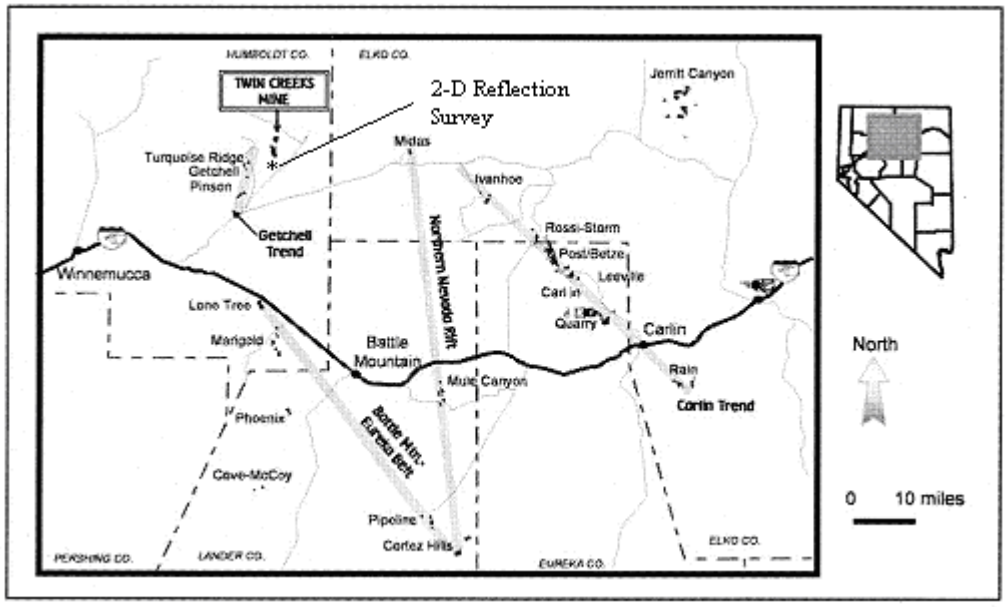

Figure 6.1.1- Map of the area around Twin Creeks Mine, Nevada with major structural trends and geological locations defined. The 2-D reflection survey was located two miles south of the open mines, as indicated on the map (after Breit et al., 2007).

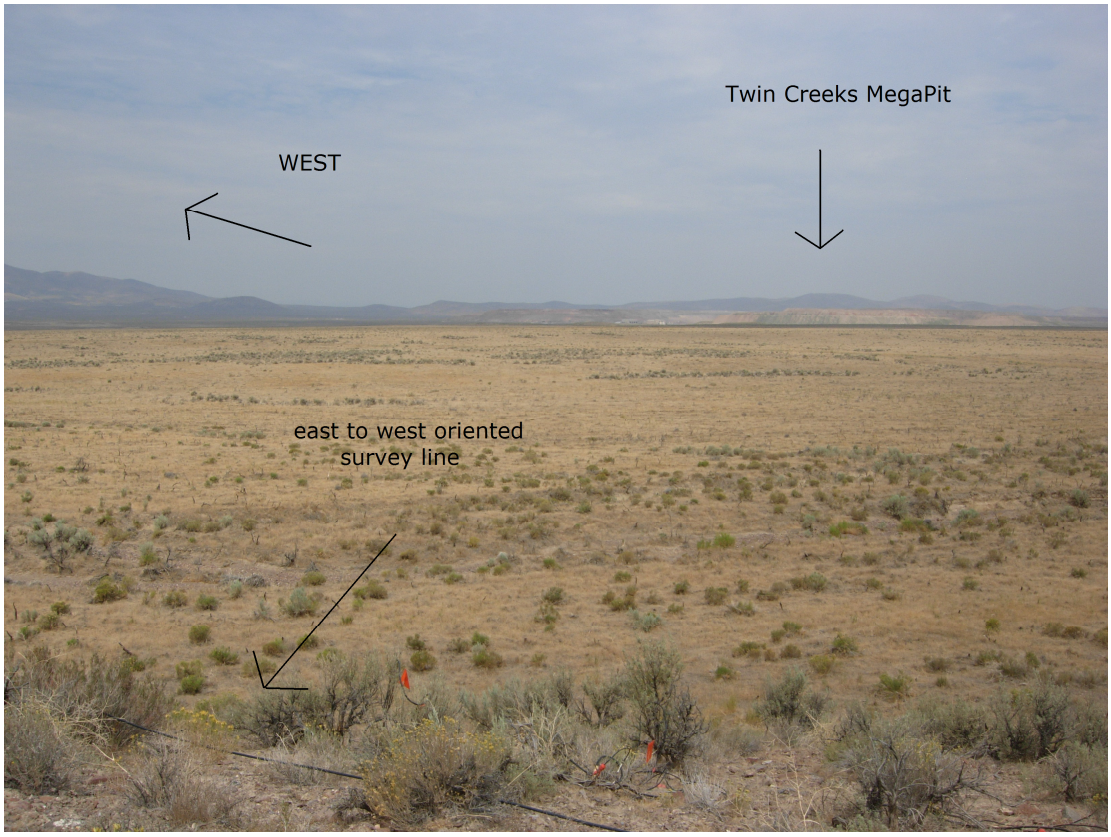

Figure 6.1.2- Site of Twin Creeks 2-D reflection survey in Humboldt County, NV. The station flags can be seen at the bottom of the picture and Twin Creeks MegaPit is located approximately 2 miles north-northwest of the survey site. The surface topography is flat at the survey site. The Dry Hills Range can be seen on the west side.

section because of the close proximity of the survey site and the cross-section (Figure 6.1.3). The unconsolidated portion of this valley contains extreme velocity variability both laterally and vertically with structurally altered carbonate basement rock, making it a seismic headache but ideal for statics research using refraction tomography.

6.2 Seismic Acquisition and Processing

A 2-D CMP line was collected 2 miles south of the Twin Creeks Mine, which was oriented east to west and designed to intersect north-south striking basin-bounding faults and image suspected intrabasin structures proposed to be associated with intrusives. The 3 miles of data were acquired using a rolling fixed-spread shot/receiver geometry with 240 live receivers recorded per shot. The receivers were three Mark Products 10 Hz geophones and the source was a 13,000 lb. IVI Minivib II imparting a 10 s long, 15-180 Hz upsweep. Geometrics Strataview seismograph controlled by a Geometrics Stratavisor recorded 12 s of data at a sampling rate of 1 ms. The receiver interval was 8 feet[5] with a 3-geophone array spaced 1 foot apart. Three shots were delivered at every other station (a 16 foot shot interval).

The data were processed to create a baseline stack using a customized flow (Figure 3.2.3), with WinSeis Turbo, LwSeis, and SurfSeis software packages. Key during this processing was generation of an AUTS coefficient for comparison with the data set processed using the same flow but including iterative vertical tomostatics.

[5] The tomography program requires the same units as the station spacing (feet). For convenience, all other values in this section are converted to feet for consistency.

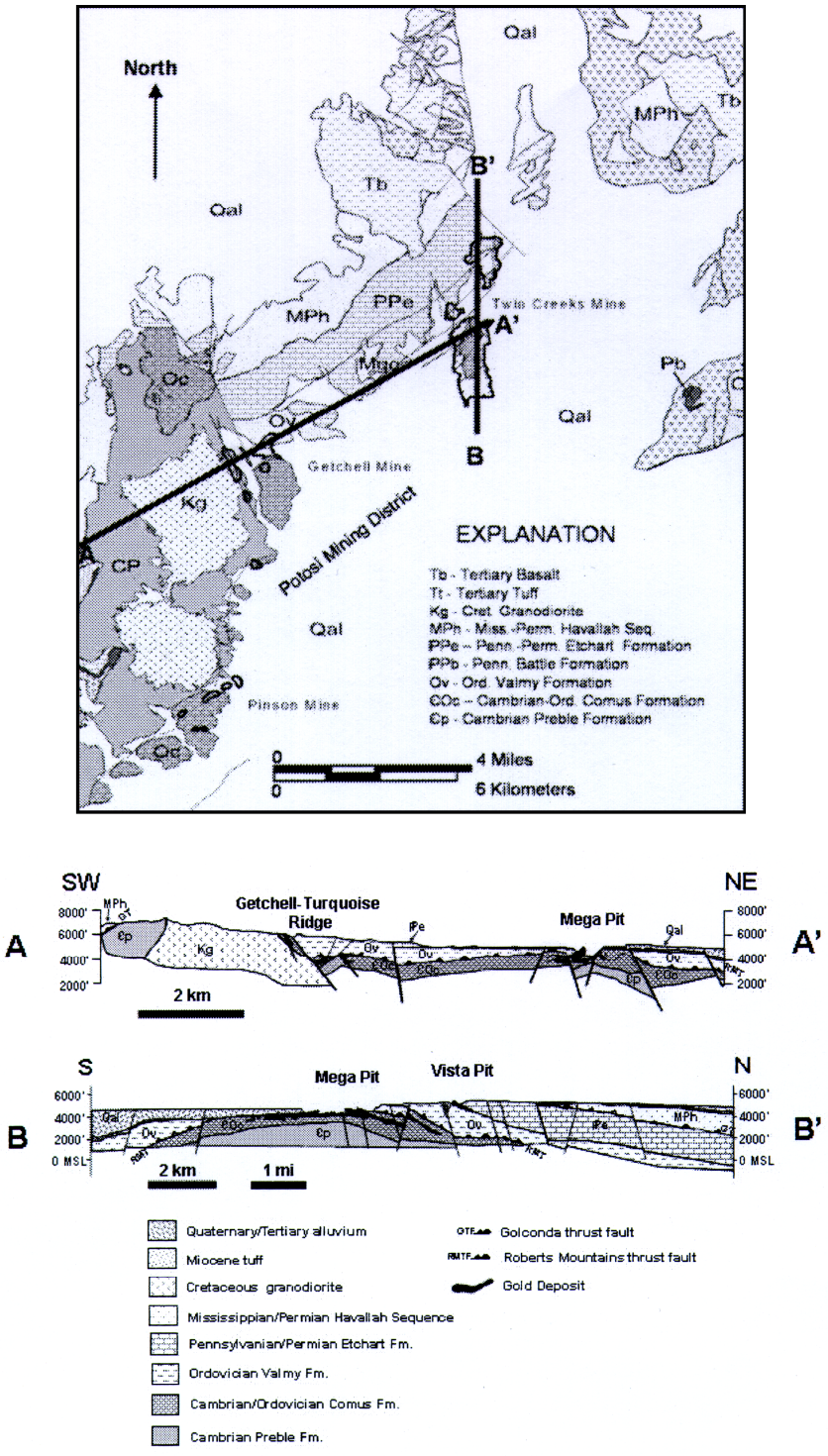

Figure 6.1.3- Regional geology near the Twin Creeks Mine. The study area is located two miles south of the mine, near the south end of the B-B' cross-section line (after Breit et al., 2007).

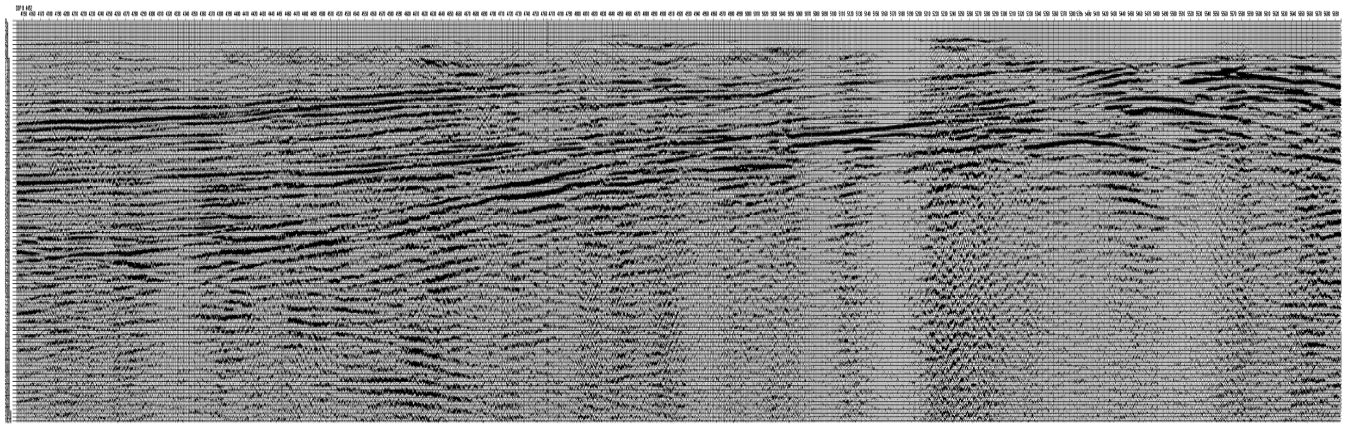

Figure 6.2.1- Stacked section of the second 1.5 mile portion of data collected at Twin Creeks, NV. The data was processed using conventional techniques, and reveals apparent west-dipping monoclinal structure on the right hand side of the image. This is plausible as seen in the folding and faulting of the Paleozoic units from Figure 5.1.2.

The stacked data possesses good reflection events and structure down to 700 ms with westward-dipping reflections at the east end of the line (Figure 6.2.1). After the final iteration of tomostatic, as determined using AUTS coefficients, the reflection coherency of the two separately processed data sets were compared with differences obvious.

The first step in the proposed tomostatic approach was to identify a viable initial model by testing tomographic smoothing parameters using TomSeis with a correlation routine. For these data three different types of smoothing were applied producing a total of 28 unique models: 1st order smoothing in the horizontal direction, 2nd order smoothing in the horizontal direction, and 2nd order smoothing in both directions (Table 6.2.2). As with the Hutchinson data smoothing tests, all parameters were kept constant. The stopping RMS was chosen to be 9 ms, 2.5% of the longest traveltime, so any solution that did reach this was not considered. Based on trends for each type of smoothing (Figure 6.2.3), and on average the 1st order horizontal smoothing shows the lowest overall AUTS coefficients. The solution with the lowest AUTS coefficient (Table 6.2.2) had a 1st order horizontal smoothing of 4000 with an AUTS coefficient of 2299.5 (the scaling factor was 33) (Figure 6.2.4).

This model is unique in that it shows vertically and laterally varying structure that is geologically reasonable because of the extent of structural deformation in the area, unlike most other solutions generated from the smoothing test. The raypath diagram shows where the problem is partially determined because of lack of ray coverage below 250 feet. Consequently, the datum chosen during the smoothing test

Smoothing							
Horizontal	Vertical	Order	# of iterations	Total	Near-offset	# of bad correlations	**AUTS** coefficient
10	10	2	6	7.06	6.05	80968	2453.5
10		2	7	22.51	14.64		
10		1	7	12.51	9.71		
1000	1000	2	2	7.92	8.02	77926	2361.3
1000		2	3	8.21	6.37	77706	2354.7
1000		1	4	7.7	5.92	76812	2327.6
1500	1500	2	7	8.67	8.92	76953	2331.9
1500		2	5	7.19	5.54	77826	2358.3
1500		1	7	8.94	6.64	76444	2316.4
2000	2000	1	7	19.24	20.05		
2000	2000	2	7	9.42	9.94		
2000		2	4	7.88	5.83	76461	2317
2000		1	3	7.74	6.8	76270	2311.2
2500	2500	2	7	10.09	10.74		
2500		2	5	7.38	6.03	76203	2309.2
2500		1	3	8.13	7.07	76470	2317.3
3000	3000	2	7	11.02	11.47		
3000		2	3	8.01	6.53	76432	2316.1
3000		1	7	10.84	7.83		
3500	3500	2	7	11.51	12.05		
3500		2	3	8.29	6.67	76838	2328.4
3500		1	5	8.07	7.05	76007	2303.2
4000	4000	2	7	11.89	12.5		
4000		2	3	7.3	6.4	76555	2319.9
4000		1	3	8.21	7.23	75884	2299.5
4500	4500	2	7	12.16	12.89		
4500		2	3	8.07	6.79	75996	2302.9
4500		1	4	8.11	7.17	76050	2304.5

Table 6.2.2- Table showing **AUTS** coefficient values (far right) for each set of smoothing parameters. Rows with no AUTS coefficients are bad models with an RMS over 9 ms. If no vertical smoothing is shown, no vertical smoothing was applied during that test. The bolded box represents the lowest AUTS coefficient with a 1st order horizontal smoothing of 4000.

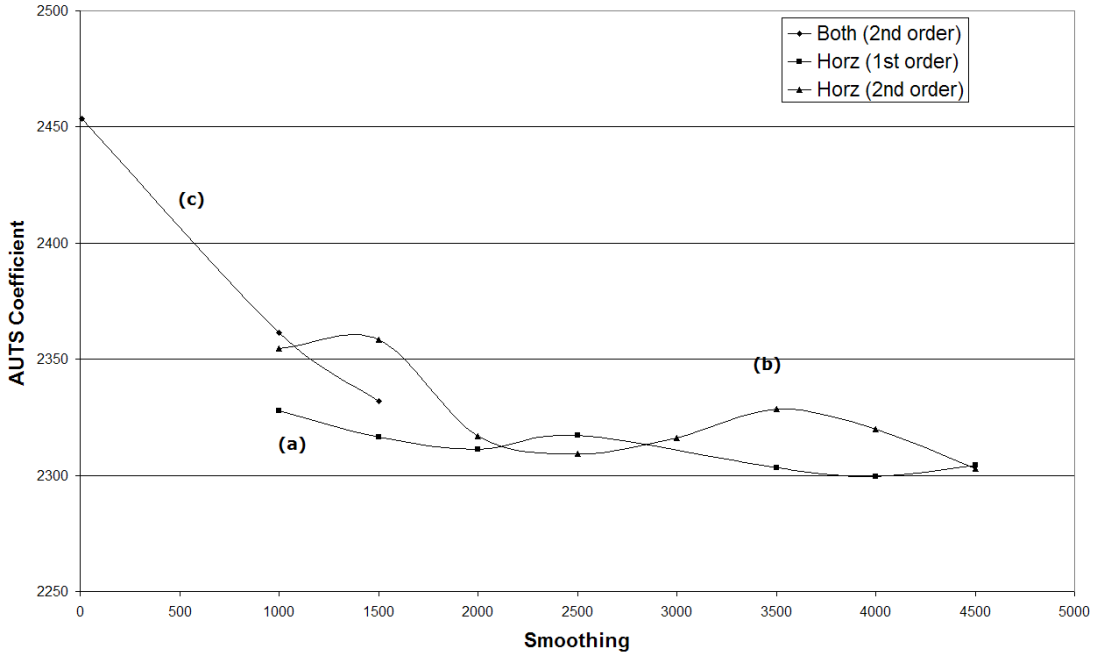

Figure 6.2.3- Diagram showing smoothing trends for each type of regularization applied in Table 6.2.2. The lowest overall was 1st order smoothing in horizontal direction (a), with 2nd order horizontal smoothing averaging highest overall (b), and 2nd order in both directions inconclusive due to lack of useable models (c).

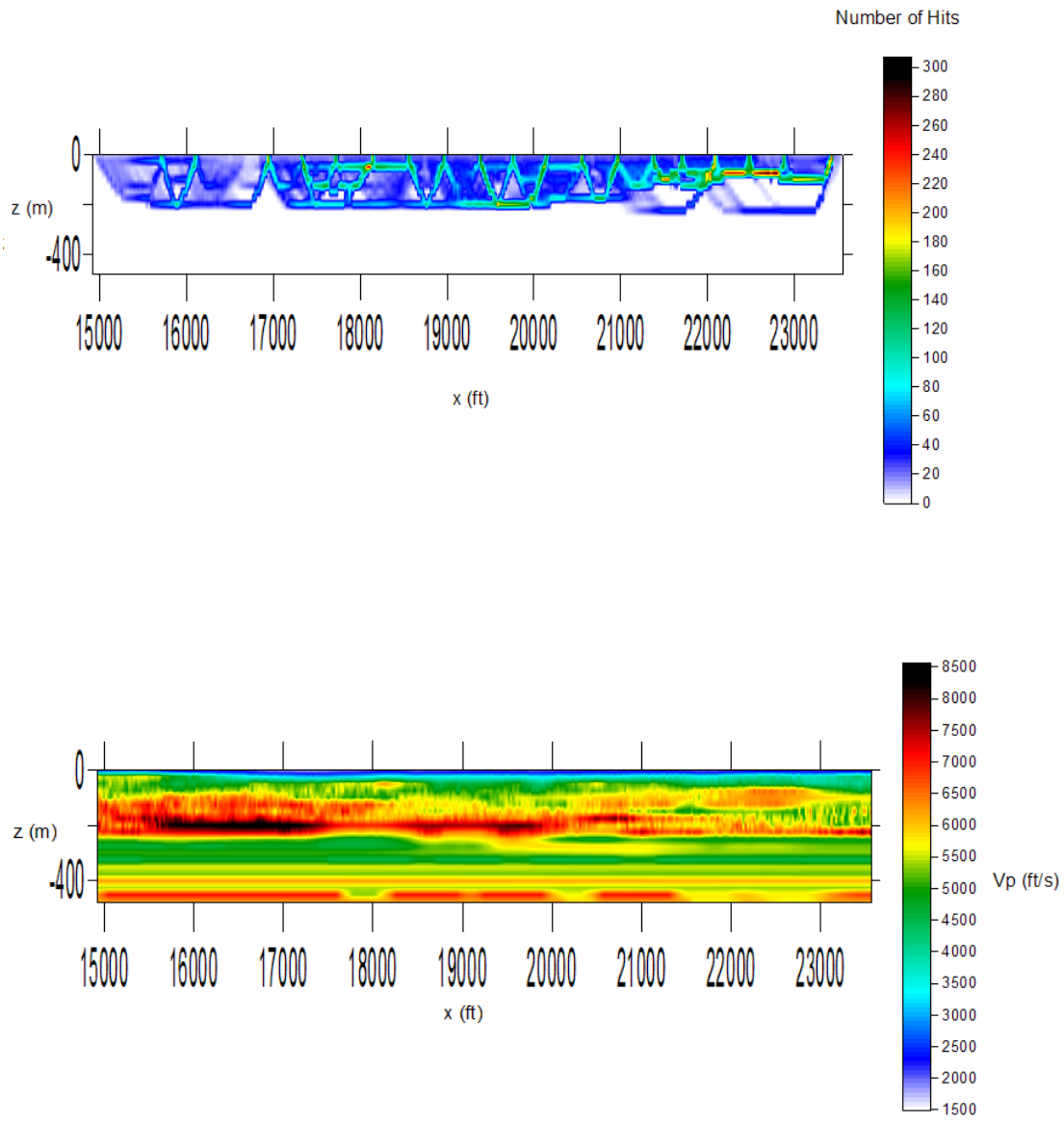

Figure 6.2.4- The model with the lowest AUTS coefficient from smoothing test is shown on bottom with the raypath diagram shown on top. The model has a horizontal smoothing of 4000, 1st order. There is evidence of structure between 20 and 220 feet deep that varies laterally across the image.

for the tomostatic corrections within the models was 240 feet. This datum was selected because all models demonstrated penetration to this depth (Figure 6.2.4).

The vertical tomostatic correction was applied to this data using the best initial model (Figure 6.2.4), first-arrivals repicked, and inverted to iterate into the next tomographic model. Once the initial model is chosen based on the smoothing tests, it becomes the *a priori* model with a damping parameter to be used during each tomographic inversion to guide the output. For these data the third iteration of tomography produced an image (Figure 6.2.5) that is smooth and maintains the structures seen between 20-220 ft. High velocity lenses that appear embedded in the model are better resolved with each iteration. These could be basalt or limestone clasts, which are found locally in the area (Breit et al., 2007).

An optimized model was reached for this data set on the 4th iteration of tomography as indicated by the AUTS coefficient dropping to low value and then sharply increasing for two iterations (Figure 6.2.6). This model resembles earlier iterations that are characterized by small changes in the high-velocity lenses (Figure 6.2.7). When this model is applied to the Twin Creeks data via vertical tomostatics, however, it substantially increased trace-to-trace reflection coherency. The tomographic model produced on the 6th iteration has a lower velocity medium with fewer high-velocity features, that also appear to be smaller (Figure 6.2.8).
The overall trend shows an optimization of the velocity model and therefore the static correction on the 4th iteration.

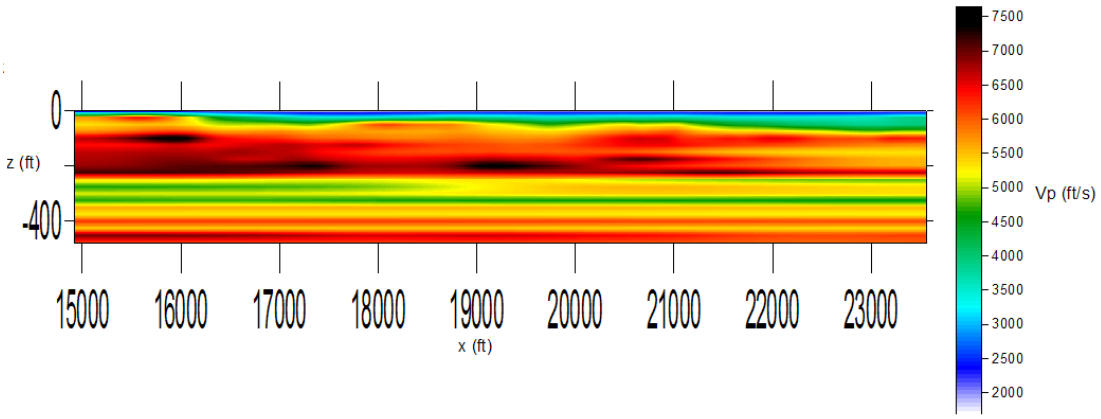

Figure 6.2.5- The tomographic image produced on the 3rd iteration of tomostatics. The overall structure is consistent, however, the model is more smoothed. There are high velocity lenses between 20 and 220 ft.

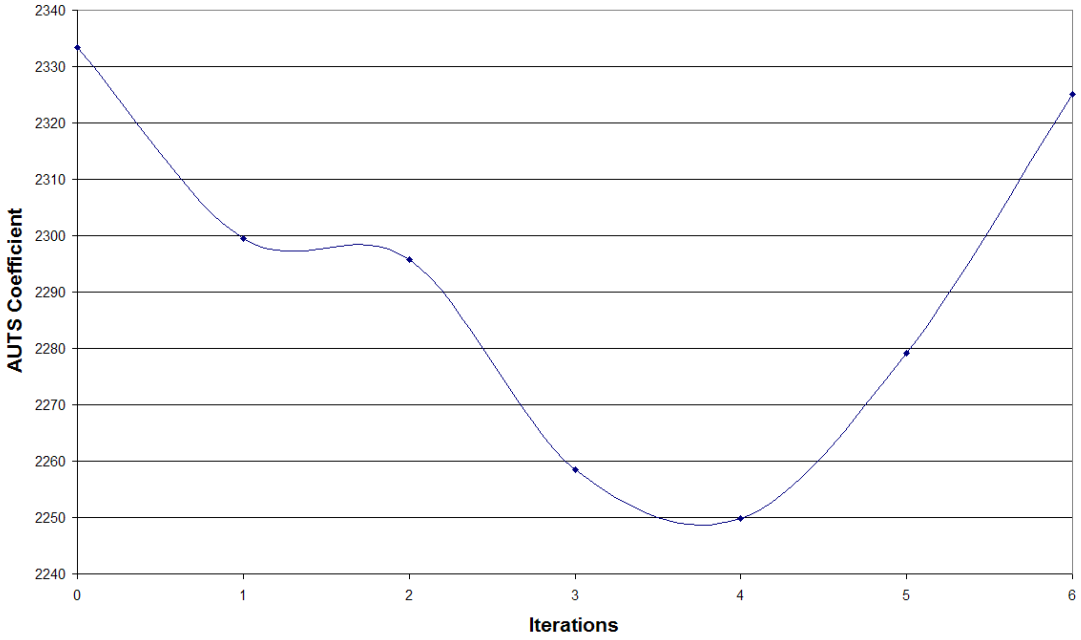

Figure 6.2.6- Graph showing trend of the AUTS coefficient for vertical tomostatics on Twin Creeks data with each iteration. The first 4 iterations show a decrease in the AUTS coefficient followed by a sharp increase on the 5th and 6th iteration. This indicates the model and the tomostatic correction are optimized on the 4th iteration.

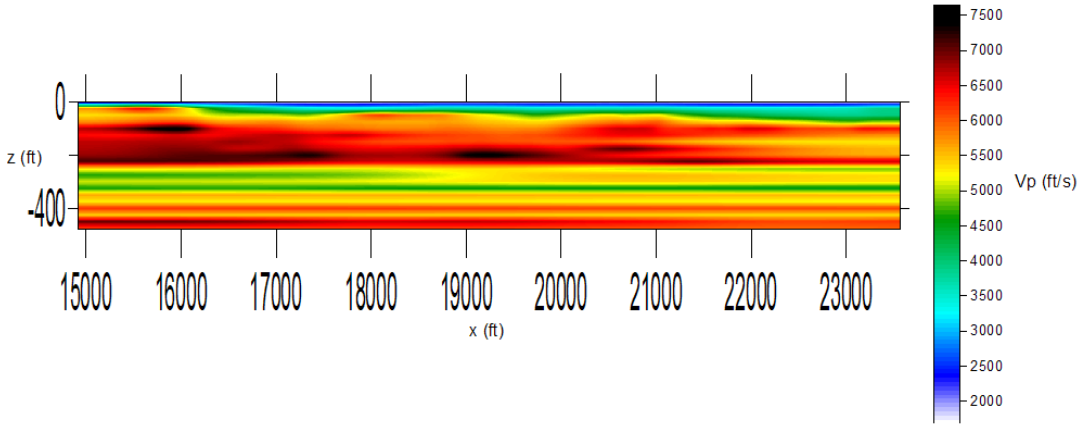

Figure 6.2.7- The model generated from the 4th iteration of tomography. This model represents the optimized velocity field decided by the resulting increase in reflection coherency, or decrease in the AUTS coefficient, from the AUTS routine.

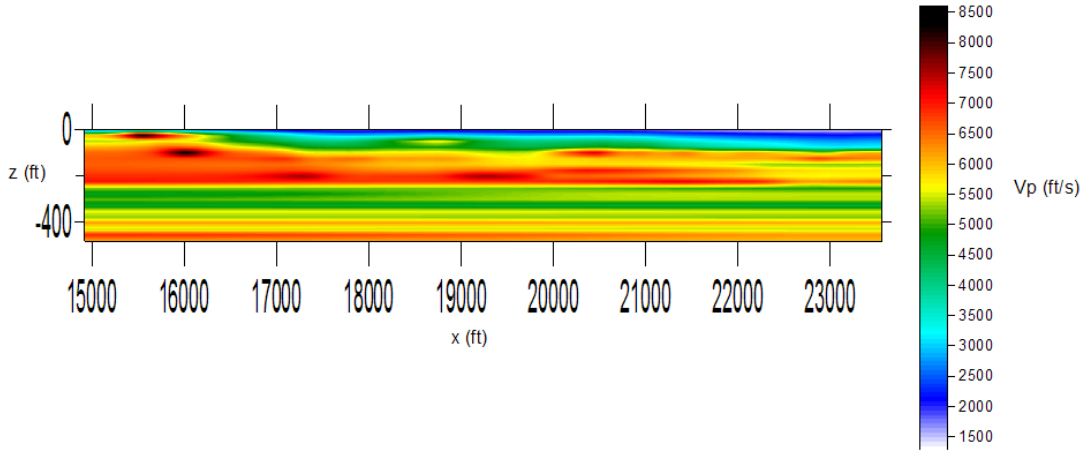

Figure 6.2.8- Tomographic model produced on the 6th iteration of tomostatics applied to the Twin Creeks data.

6.3 Discussion

An improvement in reflection coherency can be seen on Twin Creeks section after application of iterative tomostatics (Figure 6.3.1). The AUTS coefficient allowed successful convergence to a geologically viable initial model and showed an overall improvement in static corrections applied by tomostatics via the iterative approach. The optimization of a near-surface velocity model was determined to be the 4^{th} iteration of tomostatics (Figure 6.2.7) because the reflection coherency of the target reflection event decreased for the two following iterations (Figure 6.2.6). The final (6^{th}) iteration produced a velocity model that is less geologically plausible, as measured from trace-to-trace reflection coherency, than the 4^{th} iteration.

The correlation routine, although useful in eliminating residual chatter using a large time gate, has great potential as a powerful assessment tool to tackle the problem of non-uniqueness when using turning-ray tomography to perform static corrections. The method of velocity model optimization through iterative tomostatics is especially useful when applied to sedimentologically and structurally diverse areas of the world, and has shown to enhance the near-surface of the final stacked section in these areas.

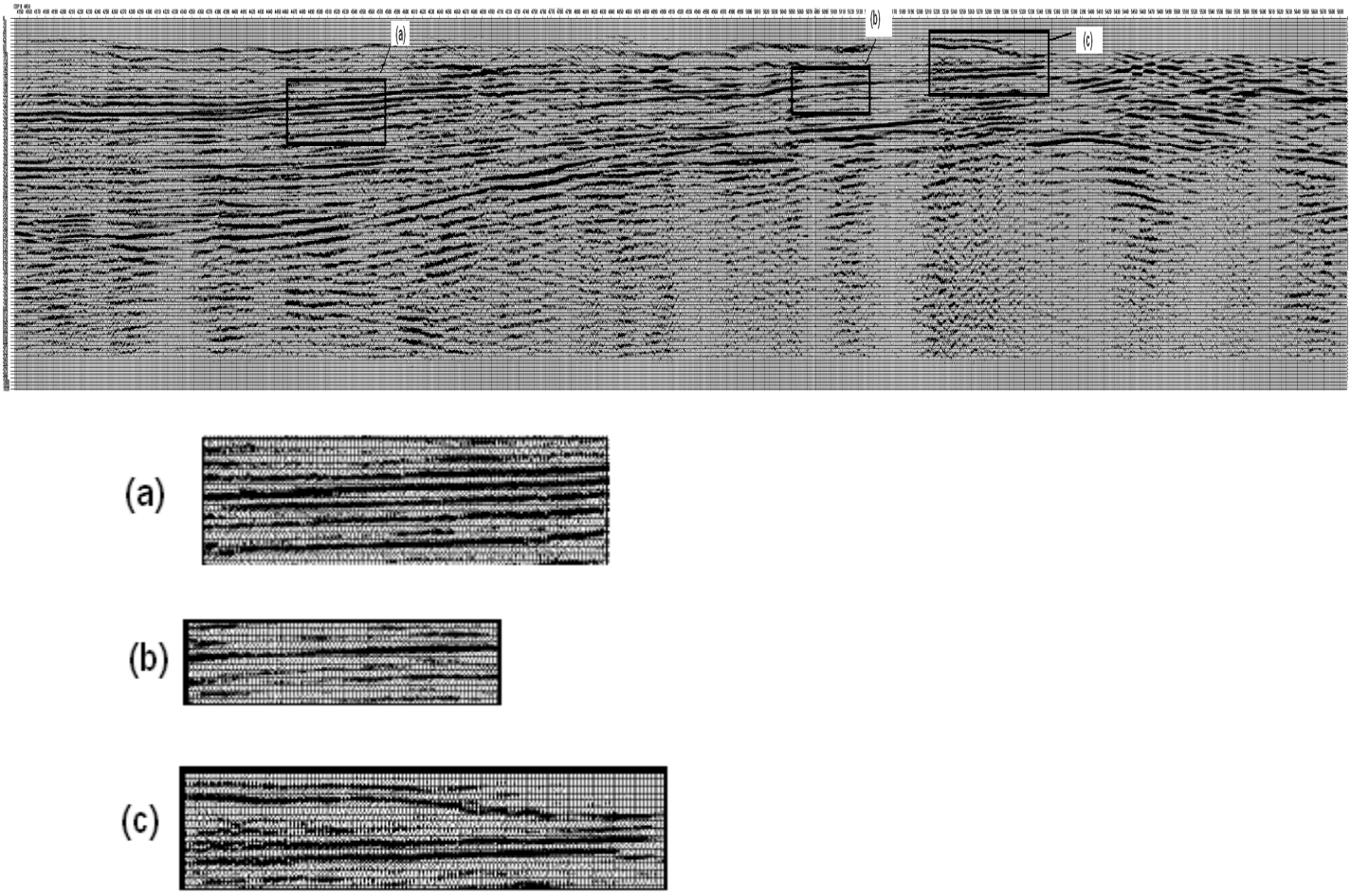

Figure 6.3.1- Final stacked section of data after iterative vertical tomostatics. The reflection coherency did increase both visually (a, b, and c) and analytically following iterative vertical tomostatic corrections.

7. Conclusions

Vertical tomostatics can be more effectively used to optimize the velocity model and static correction in highly weathered areas if the near-surface model is constrained by calculation of AUTS coefficients for each iteration. Surface consistent statics successfully measured an increase in trace-to-trace reflection coherency in specific events, with improvement in the tomographic velocity model. Correlation statics using the AUTS coefficient is a powerful tool for identifying an initial tomographic model through smoothing tests, and also to gauge improvement with each iteration of tomostatics applied to the data.

This method is beneficial to the final stacked section of any survey because of enhanced near-surface velocity characterization, however it is time-consuming. Depending on the complexity of the first-arrivals and the cell size of the tomography, tomographic software can take hours to run, so this method is especially time inefficient during the smoothing tests. The Twin Creeks survey site is stratigraphically complicated making an improvement on the near-surface velocity model important and justifying this costly approach. The subsurface near Hutchinson, KS is more straightforward, so the advantages presented by the iterative tomostatic approach applied to these data are less obvious. The time cost should be considered against the complexity of the area before implementing this method.

Angle-dependent tomostatics appears not to be a valid approach in this study. The lack of success in this study is likely due to an inadequate algorithm or gridding assumptions that were used to calculate average velocity and raypath length. The

raypath model may also be too simplistic to account for spherical divergence of the wavefield after encountering anomalies, as seen with the synthetic data. Further investigation into the relationship between the physical size of the velocity irregularity and the interaction with the Fresnel zone of the input energy would be beneficial.

Future work on this approach is needed to explore the 3-dimensional aspect of near-surface velocity characterization and tomostatics application to 3-D datasets. The angle-dependent approach may be viable if more attention is paid to the algorithm for velocity calculation through each cell of tomographic model, and application of the resulting times as a floating point number, as opposed to an integer, for better resolution. The offset-dependence is a problem that could be addressed by applying the static correction to CMP's during the NMO-correction.

References

Bayne, C. K., 1956, Geology and Ground-water Resources of Reno County, Kansas, accessed 30 April 2008; http://www.kgs.ku.edu/Hydro/Hutch/GeneralGeology/.

Berkhout, A. J. and D. J. Verschuur, 2001, Seismic imaging beyond depth migration: Geophysics, **66**, 1895-1912.

Bevington, P. R., and D. K. Robinson, 2003, Data Reduction and Error Analysis in the Physical Sciences, 3rd Edition: McGraw-Hill Book Co.

Bishop, T. N., K. P. Bube, R. T. Cutler, P. L. Langan, P.N. Love, J. R. Resnick, R. T. Shuey, D. A. Spindler, and H. W. Wyld, 1985, Tomographic determination of velocity and depth in laterally varying media: Geophysics, **50**, 903-923.

Breit, F. J., M. W. Ressel, S. D. Anderson, and E. M. Muirhead, Geology and Gold Deposits of the Twin Creeks Mine, Humboldt County, NV, Report by Newmont Mining Corporation, received June 2007.

Carmichael, R. S., 1990, CRC practical handbook of physical properties of rocks and minerals: CRC Press, Inc.

Carter, N. L., and F. D. Hansen, 1983, Creep of rock salt: Tectonophysics, **92**, 275-333.

Cox, M., 1999, Static Corrections for Seismic Reflection Surveys: Society of Exploration Geophysicists.

de Amorim, W. N, P. Hubral, and M. Tygel, 1987, Computing field statics with the help of Seismic Tomography: Geophysical Prospecting, **35**, 907-919.

Dines, K. A., and R. J. Lytle, 1979, Computerised geophysical tomography: Proc. IEEE, **67**, 1065-1073.

Disher, D. A., and P. J. Naquin, 1970, Statistical automatic statics analysis: Geophysics, **35**, 574-585.

Dobrin, M. B., 1976, Introduction to geophysical prospecting: McGraw-Hill Book Co.

Edge, A. B., and T. H. Laby, 1931, The principles and practice of geophysical prospecting: Cambridge University Press.

Gardner, L. W., 1939a, An areal plan of mapping subsurface structure by refraction shooting: Geophysics, **4**, 247-259.

Garotta, R., and D. Michon, 1968, Static corrections in reflection seismology: Presented at 13th Annual International Meeting, EAEG.

Hagedoorn, J. G., 1956, The plus-minus method of interpreting seismic refraction sections: Geophysical Prospecting, **7**, 158-182.

Hatherly, P. J., M. Urosevic, A. Lambourne, and B. J. Evans, 1994, A simple approach to calculating refractions statics corrections: Geophysics, **59**, 156-160.

Hileman, J. A., P. Embree, and J. C. Pflueger, 1968, Automated Statics Corrections: Geophysical Prospecting, **16**, 326-358.

Hunter, J. A., S. E. Pullan, R. A. Burns, R. M. Gagne, and R. L. Good, 1984, Shallow seismic reflection mapping of the overburden□bedrock interface with the engineering seismograph—Some simple techniques: Geophysics, **49**, 1381-1385.

Ivanov, J., R. D. Miller, J. Xia, D. Steeples, and C. B. Park, 2005, The inverse problem of refraction travel times, Part I: Types of geophysical nonuniqueness through minimization: Pure and Applied Geophysics, **162**, 447-459.

Ivanov, J., R. D. Miller, J. Xia, D. Steeples, and C. B. Park, 2005, The inverse problem of refraction travel times, Part II: Quantifying refraction nonuniqueness using a three-layer model: Pure and Applied Geophysics, **162**, 461-477.

Ivansson, S., 1985, A study of methods for tomographic velocity estimation in the presence of low-velocity zones: Geophysics, **50**, 969-988.

Irvine, B. M., and J. K. Worley, 1969, The application and limitations of automatic residual static correction techniques: Presented at 39th Annual International Meeting, SEG.

Lo, T. W., and P. Inderwiesen, 1994, Fundamentals of seismic tomography: Society of Exploration Geophysicists.

Menke, W., 1984, Geophysical Data Analysis: Discrete Inverse Theory: Academic Press, Inc.

Merriam, D. F., and C. J. Mann, 1957, Sinkholes and related geologic features in Kansas: Transactions Kansas Academy of Science, **60**, 207-243.

Meju, M., 1994, Geophysical Data Analysis: Understanding Inverse Problem Theory and Practice: Society of Exploration Geophysicists.

Miller, R. D., 2006, High-resolution seismic reflection to identify areas with subsidence potential beneath U.S. 50 highway in eastern Reno County, Kansas: Presented at 19th Annual Meeting, SAGEEP.

Miller, R. D., 2007, Shallow seismic to characterize extreme weathered layer variability, Newmont Mining Corporation Project Proposal.

Nolet, G., 1987, Seismic Tomography: D. Reidel Publishing Co.

Palmer, D., 1980, The generalized reciprocal method of seismic refraction interpretation: Society of Exploration Geophysicists.

Pugin, A. and S. E. Pullan, 2000, First-arrival alignment static corrections applied to shallow seismic reflection data: Journal of Environmental and Engineering Geophysics, **5**, 7-15.

Sherwood, J. W. C., and J. Donaldson, 1970, Automatic residual static corrections: Presented at the 40th Annual International Meeting, SEG.

Sheriff, R. E., 2002, Encyclopedic Dictionary of Exploration Geophysics: Society of Exploration Geophysicists.

Simmons, J. L., Jr., and M. M. Backus, 1992, Linearized tomographic inversion of first-arrival times: Geophysics, **57**, 1482-1492.

Steeples, D. W., R. D. Miller, and R. A. Black, 1990, Static corrections from shallow-reflection surveys: Geophysics, **55**, 769-775.

Stefani, J. P., 1993, Possibilities and limitations of turning-ray tomography: a synthetic study: 63rd Annual International Meeting, SEG, Expanded Abstracts, 610-612.

Stewart, R. R., 1991, Exploration seismic tomography: Fundamentals: Society of Exploration Geophysicists.

Taner, M. T., F. Koehler, and K. A. Alhilali, 1974, Estimation and correction of near-surface time anomalies: Geophysics, **39**, 441-463.

Taner, M. T., D. E. Wagner, E. Baysal, and L. Lu, 1998, A unified method for 2-D and 3-D refraction statics: Geophysics, **63**, 260-274.

Taner, M. T., 1998, The dynamics of statics: 68th Annual International Meeting, SEG, Expanded Abstracts, 1409 – 1412.

Taner, M. T., A. J. Berkhout, S. Treitel, and P. G. Kelamis, 2007, The dynamics of statics: The Leading Edge, **26**, 396-402.

Tikhonov, A. N., and V. Y. Arsenin, 1977, Solutions of Ill-Posed Problems: John Wiley and Sons.

Vireux, J., 1986, P-SV wave propagation in heterogeneous media: Velocity-stress finite-difference method: Geophysics, **51**, 889-901.

Wong, J., N. Bregman, G. West, and P. Hurley, 1987, Cross-hole seismic scanning and tomography: The Leading Edge, **6**, 36-41.

Walters, R. F., 1978, Land subsidence in central Kansas related to salt dissolution: Kansas Geological Survey Bulletin 214, 1-32.

White, D. J., 1989, Two-dimensional seismic refraction tomography: Geophysics Journal, **97**, 223-245.

Xia, J., Y. Xu, R. D. Miller, and C. Zeng, 2009, A trade-off solution of regularized geophysical inversion using model resolution and covariance matrices: Presented at 22nd Annual Meeting, SAGEEP.

Yilmaz, O., 1987, Seismic Data Processing: Society of Exploration Geophysicists.

Zeng, C., J. Xia, and R. D. Miller, 2009, Estimation of absorbing boundary parameters for near-surface seismic modeling: Presented at 22nd Annual Meeting, SAGEEP.

Zhu, X., and G. A. McMechan, 1988, Estimation of near-surface velocities by tomography: 58th Annual International Meeting, SEG**,** Expanded Abstracts**,** 1236-1238.

Zhu, X., D. P. Sixta, and B. G. Angstman, 1992, Tomostatics: Turning-ray tomography + static corrections: The Leading Edge, **11**, 15-23.

Zhu, X., D. P. Sixta, and B. G. Angstman, 1992, Seismic Processing II: Estimation of Statics: 62nd Annual International Meeting, SEG, Expanded Abstracts, 1108-1111.

Appendix A

Residual statics routines rely on a cross-correlation function to gauge the similarity between two waveforms. In the automatic statics calculation or AUTS routine the cross-correlation function is given a gate to examine reflections, whereas with trim statics the cross-correlation function examines two entire traces in time-varying manner and aligns them. For two waveforms *G(t)* and *H(t)*, the normalized cross-correlation function $\phi_{GH}(\tau)$ is a given as a function of the time shift, τ, between the functions by

$$\phi_{GH}(\tau) = \frac{\int_{-\infty}^{\infty} G(t)H(t+\tau)dt}{\int_{-\infty}^{\infty} G(t)dt \int_{-\infty}^{\infty} H(t)dt}.$$

The denominator is the normalizing factor, and when normalized a cross-correlation of 1 indicates a perfect match, 0 indicates little correlation, and negative values indicate inverted wavelets (Sheriff, 2002). A normalized cross-correlation is called a correlation coefficient and that value is associated with each comparison between the pilot trace and the time-shifted trace. The cross-correlation coefficient must reach a threshold or it is considered a failed match and no shift will take place.

Appendix B

Vertical Datum Tomostatic Program

```
//---------------------------------------------------------------------------
#include <iostream>
#include <conio.h>
#include <fstream>
#include <string>
#include <vector>
#include <stdio.h>
#include <math.h>
#define MAXWORDSIZE    256

#pragma hdrstop
using namespace std;
//---------------------------------------------------------------------------

#pragma argsused
double **V=NULL;
int grd();

int main()
{
char inpVelFile[50], inpDataFile[50], outDataFile[50], TempChar='\0', *WordBuffer ;
short inhead, outhead, spareHead,*headerInp;
short headerTemp[120];
int header92, header19, header35, headercount=0, samplecount=0, ref_vel, shotnumber;
int a, b, c, d, trace, file, noFiles, noTraces, noSamples, totalNumSamp, totalNumHead ;
```

```
int header86, header87, y1, y2, header82, header83, kr, ks, kr_start, ks_start, stopcell;
float x_max, x_min, z_max, z_min, v_min, v_max;
float *dataTemp, *dataInp, depth, datum, ratio, cellsize;
float loc_s, loc_r, s1, s2, offset, kr_float, ks_float;

//open kgs file-------------------------------------------------------------------

cout<<"Enter a kgs (.dat) file:  ";
cin>>inpDataFile;
//cout<<"Enter total number of traces (traces/record * # of records):   ";
//cin>>noTraces;
cout<<endl<<inpDataFile<<endl<<noTraces<<" traces"<<endl;
FILE * p2file;
p2file = fopen(inpDataFile, "rb");

//-----------open velocity file for use later----------------------------------
cout<<"Enter a velocity (.grd) file:  ";
cin>>inpVelFile;
cout<<endl<<inpVelFile<<endl;
cout<<"Enter cellsize of velocity file: ";
cin>>cellsize;
cout<<endl<<"Enter datum in units of velocity file (must be a multiple of cellsize):";
cin>>datum;
stopcell = (int) ceil (datum/cellsize);
FILE * pfile;
pfile = fopen (inpVelFile, "rt"); //open velocity file

//---------------open file to write data to-------------------------------------

cout<<"Enter output file name:  ";
cin>>outDataFile;

FILE * p3file;
p3file = fopen(outDataFile, "wb");

//int grd();
//{

int CharNumber=0, DigitalWordNumber=0, digitalflag=0;
int j=0, k=0, J, K;
long begin, end;
float  DebugVar=0.0;
string mystr;

      if (pfile!=NULL)
            {
            WordBuffer = new char [MAXWORDSIZE];
            WordBuffer[0]='\0';
            while (! feof (pfile) )
            {
               if (j<0) {break;}
               TempChar=fgetc(pfile);  //input velocity file
               switch (TempChar)
```

```
                {
                 case ' ':
                 case ',':
                 case '\n':
                 case '\t':

                 if(CharNumber!=0)  //check to see which char
                 {
                    WordBuffer[CharNumber]='\0';
                    if (digitalflag==1)
                    {
                      DigitalWordNumber++;
 /* count velocities*/       //cout<<endl<<DigitalWordNumber<<endl;
                      CharNumber=0;
/*Convert ascII to float*/   DebugVar=atof(WordBuffer);

                      if (DigitalWordNumber<9)
                      {
                        switch(DigitalWordNumber)
                        {
                          case 1:
                            K=(int) DebugVar;
                            break;
                          case 2:
 /*2-D Velocity Array*/              J=(int) DebugVar;
                            V=new double * [J+1];
                            for (int count=0;count<J;count++)
                            {
                              V[count]=new double[K+1];
                            }
                            k=K-1; j=J-1;
                            break;
                          case 3:
                            x_min=(float)DebugVar;
                            break;
                          case 4:
                            x_max=(float)DebugVar;
                            break;
                          case 5:
                            z_min=(float)DebugVar;
                            break;
                          case 6:
                            z_max=(float)DebugVar;
                            break;
                          case 7:
                            v_min=(float)DebugVar;
                            break;
                          case 8:
                            v_max=(float)DebugVar;
                            break;
                        }
                      }
                      else
```

```
                    {
                      if(j<0) {break;}
                      V[j][k]=DebugVar;
                      k--;
                       if(k<0)
                      {
                       j--;
                       k=K-1;
                       //cout<<endl<<V[j][k];
                      }
                    }
                  }
                }
               break;
             case EOF:
               break;
             default:
               if((isdigit(TempChar)!=0)||(TempChar=='.')||(TempChar=='-'))
               {
                 digitalflag=1;
                 WordBuffer[CharNumber]=TempChar;
                 CharNumber++;
               }
               else
               {
                 digitalflag=0;
                 CharNumber=0;
               }
               if(CharNumber>=MAXWORDSIZE||digitalflag==0)
               {
                 while((TempChar!=' ')&&(TempChar!='\n')&&(TempChar!='\t'))
                 {
                   TempChar=fgetc(pfile); //skip over remaining char
                 }
                 break;
               }
             }//end switch

          }//end while
          fclose(pfile);
          delete[] WordBuffer;
          }

     else cout<< "Unable to open file";

//       getch();
//      return 0;
//}
//---------------------------------------------------------------------------
noTraces=119040;
shotnumber=1;
trace=1;
file=1;
```

```
a=0;
headerTemp[81]=(short)0;
dataTemp=0;
//   for (a=0;a<1;a++)
{
fread (headerTemp,2,120,p2file);
noSamples  = headerTemp[57];        //get number of samples from header 58
rewind (p2file);
cout<<endl<<noSamples<<" samples per trace";
}
totalNumHead=noTraces*120;
totalNumSamp=noSamples*noTraces;
dataTemp= new float[noSamples];
dataInp= new float[totalNumSamp] ;// # traces x # samples
headerInp= new short [totalNumHead];  //traces x 120

//testing velocity grid output----------------------------------------------------

cout<<endl<<"The size of the velocity grid is "<<J<<" by "<<K<<endl;
cout<<endl<<"The datum is at cell "<<stopcell<<endl;
//-------------------------------------------------------------------------------
/*start reading from data file-> split into header and data*/

while (! feof (p2file) )
{
b=0;
for (b=0;b<noTraces;b++)
  {
  fread (headerTemp,2,120,p2file);
  fread (dataTemp,4,noSamples,p2file);
  c=0;

  for(c=0;c<120;c++)
    {
    headerInp[(((trace-1)*120)+c)]=headerTemp[c];

    d=0;
    for(d=0;d<noSamples;d++)
      {
      dataInp[(trace-1)*noSamples+d]=dataTemp[d];
      }

    }
    headerTemp[c]=headerInp[(((trace-1)*120)+c)];
    header19=headerTemp[18];    //reading header 19 and 35
    header35=headerTemp[34];

float f_header19, f_header35;        //convert to a float
    f_header19=header19;
    f_header35=header35;
    offset = f_header19/f_header35;  //offset is determined by horizontal multiplier (35)
//    cout<<endl<<"The offset for this trace is: "<<offset<<endl;
    ratio= (depth*2/offset);
```

```
//    cout<<endl<<"The ratio of depth to offset for this trace is: "<<ratio<<endl;

//read headers 82 and 83 to find minimum and maximum receiver stations----------

    header82=headerTemp[81];
    y1=header82-1;
//    cout<<endl<<"Minimum receiver stations is: "<<header82<<endl;
//    cout<<endl<<"Minimum x is: "<<x_min<<endl;
    header83=headerTemp[82];
    y2=header83;
//    cout<<endl<<"Maximum receiver station is: "<<header83<<endl;
//    cout<<endl<<"Maximum x is: "<<x_max<<endl;


//convert station to location in meters----------------------------------------

    header86=headerTemp[85];
    header87=headerTemp[86];

    s1=(y2-y1)/(x_max-x_min);    // calculate linear interpolation constant (slope)
    loc_r = ((header86-y2)/s1)+x_max;  //converted reciever location
    loc_s = ((header87-y2)/s1)+x_max;  //converted source location

//convert receiver and sources location to cell location (K)-------------------

    s2= ((x_max-x_min)/(-K)); //slope for K conversion
    kr_float = ((x_max-loc_r)/s2)+K; //converted to receiver cell
    kr = (int)ceil (kr_float);


    ks_float = ((x_max-loc_s)/s2)+K; //converted to source cell
    ks = (int)ceil(ks_float);

    kr_start= kr;
    ks_start= ks;
//    cout<<endl<<"The receiver for this trace is at "<<loc_r<<" m at the "<<
//    kr<<" cell."<<endl;

//    cout<<endl<<"The source for this trace is at "<<loc_s<<" m at the "<<
//    ks<<" cell."<<endl;

//check if offset is small enough to consider vertically incident---------------
//raypaths

    float  vr_ave, vs_ave, raypath, x, x_2, y, y_2, sum_xy;
    double sum_r, sum_s;
    float offset_check;
    offset_check=offset/(2*depth);

    int Ratio;
    Ratio=(int) ceil(ratio);

//    cout<<endl<<"Ratio= "<<Ratio<<endl;
```

```
    x= cellsize*(J/Ratio);
    x_2= pow(x,2);
    y= cellsize*stopcell;
    y_2= pow(y,2);
    sum_xy= x_2+y_2;
//    raypath = sqrt(sum_xy);  //calculate length of raypath using ratio of
                          //depth to offset
   raypath = y;

    sum_r=0;
    sum_s=0;

//    if (offset_check<.1763)
//      {
//      cout<<endl<<"vertically incident pair!"<<endl; //if vertically incident
      for (int m=0; m<stopcell; m++)            //calculate velocities directly
        {
        sum_r += V[m][kr];
        }
      for (int n=0; n<stopcell; n++)
        {
        sum_s += V[n][ks];
        }
        vr_ave=sum_r/stopcell;  //average velocity at receiver location for datum
        vs_ave=sum_s/stopcell; //average velocity at source location for datum

//calculate source and receiver static (in ms) and write into header------------

   float  tt_source, tt_receiver, total_tt ;

   tt_source = (raypath/vs_ave)*1000;
   tt_receiver = (raypath/vr_ave)*1000;
   total_tt = tt_source + tt_receiver;  //calculate static by adding source and
                                //receiver traveltime
//   cout<<endl<<"The static correction for this trace is "<<stat_corr<<" ms."<<endl;

//write to headerTemp and then output file-------------------------------------

   short source_corr, rec_corr, header50, header51, header52, stat_corr;

   stat_corr = (short)ceil(total_tt); //total static correction for each trace

   source_corr=(short)ceil(tt_source);
   rec_corr=(short)ceil(tt_receiver);

   if (rec_corr>100||rec_corr<=0)
     rec_corr= 49;   //make receiver correction default to 50 if there is a memory
                 //error with array
   if (source_corr>100||source_corr<=0)
       source_corr= 49;

   headerTemp[49]= -source_corr;  //negative shift upwards
```

```
  header50=headerTemp[49];
  if (abs(headerTemp[49])>100)
     {
     cout<<endl<<"Source static is out of range at trace "<<trace<<" = "<<headerTemp[49];
     cout<<endl<<"Source correction is: "<<source_corr<<endl;
     cout<<endl<<"Starting cell is: "<<ks_start<<endl<<"Ending cell is: "<<ks<<endl;

     getch();
     }
 //  cout<<endl<<"Receiver "<<trace<<"correction is: "<<rec_corr<<endl;
  headerTemp[50]= -rec_corr;  //overwrite previous correction!!!
  header51=headerTemp[50];
  if (abs(headerTemp[50])>100)
     {
     cout<<endl<<"Receiver static is out of range at trace "<<trace<<" = "<<headerTemp[50];
     cout<<endl<<"Receiver correction is: "<<rec_corr<<endl;
     cout<<endl<<"Starting cell is: "<<kr_start<<endl<<"Ending cell is: "<<kr<<endl;

     getch();
     }
//   headerTemp[51]= -stat_corr;
//   header52=headerTemp[51];

//   cout<<endl<<headerTemp[49]<<endl<<headerTemp[50]<<endl;




  fwrite(headerTemp,2,120,p3file);
  fwrite(dataTemp,4,noSamples,p3file);


//   cout<<endl<<trace<<endl;
//   cout<<endl<<"------------------------------------------------------------"<<endl;
  trace++;

  if ((trace%240)==0)
    {
    shotnumber++;
    cout<<endl<<rec_corr<<endl;
    cout<<endl<<source_corr<<endl;
    cout<<endl<<"--"<<shotnumber<<endl;
//     cout<<endl<<"Receiver correction: "<< header50<<endl;
//     cout<<endl<<"Source correction: "<<header51<<endl;
//     cout<<endl<<"Total correction: "<<header52<<endl;
    }
//  getch();
  }
}
fclose(pfile);
fclose(p2file);
fclose(p3file);
return 0;
```

```
delete [] dataTemp;
delete [] dataInp;
delete [] headerInp;
}
//---------------------------------------------------------------------------
```